Liquid Crystal Alignment on Embossed Polymer Films

Walter A. Schenck

A dissertation submitted to the faculty of the University of North Carolina at Chapel Hill in partial fulfillment of the requirements for the degree of Doctor of Philosophy in the Department Chemistry.

Chapel Hill
2010

Approved By:

Edward T. Samulski

Cynthia Schauer

Thomas Meyer

Valerie Ashby

Sergei Sheiko

Abstract

Walter A Schenck: Liquid Crystal Alignment on Embossed Polymer Films
"(Under the direction of Edward T Samulski)"

Liquid Crystal Displays, LCDs are ubiquitous. At the heart of the display is a polymer film which is used to uniformly align the liquid crystal over large areas—the dimensions of the LCD itself. First generation alignment layers consist of rubbed PI films fabricated by a mechanical rubbing process which produces dust and mechanical damage that is not consonant with clean room fabrication. Furthermore, the mechanism of liquid crystal alignment on rubbed surfaces is poorly understood. The ability to understand the alignment mechanism and develop novel alignment layers may lead to more efficient devices and manufacturing processes.

In this work we employed soft lithography as an alternative fabrication method of liquid crystal alignment layers. We study the mechanism of liquid crystal alignment on polymer films with variable feature dimensions. One dimensional line gratings were used to examine the mechanism of liquid crystal alignment on rubbed surfaces. We determined that the physical topography is sufficient to align the liquid crystal director; however, the chemical interaction between the mold and the alignment layer during fabrication can affect the orientation of the director. If this fabrication method is to be used, either the mold should be removed in a manner that reinforces alignment induced by the surface topography, or the mold and alignment layer chemistry must be optimized to prevent any unwanted interactions. We also fabricated alignment layer features exhibiting four-fold (square and rectangular

patterns), six-fold (triangles in a hexagonal array), and five-fold (Penrose aperiodic patterns) symmetries. We observed multi-stable alignment on such surfaces and observed that pattern features less than 100nm tall and about 500nm in- plane width have the best optical uniformity.

Acknowledgements

I would like to thank my advisor Ed Samulski for his patience and support during my time at UNC. He has always had one more idea for me to try when I thought I had run out of ideas and was ready to give up. I would like to thank Doo-Hyun Ko for being willing to share his knowledge of LCDs with me. I would like to thank the other members of the Samulski lab with whom I was able to experience this challenging and eye opening time of life. I would also like to thank Noreen Durkin for creating some of the graphic art used in this dissertation.

I would like to thank my wife Shawntel for being willing to move across the country, far away from family, with our newborn girl, and start a new part of our life together. You helped to keep me stay focused on the important things in life and helped to establish the balance between family and work that is so easily lost in this world. Somehow we managed to stay relatively sane while raising our kids and trying to graduate. I love you.

Finally, I would like to thank my parents for being supportive and allowing me to find my own path. They raised me in an environment that allowed me to determine my own success or failure and because of that I have learned much in life.

Table of Contents

List of Tables

Table of Figures

List of Abbreviations and Symbols

AFM	atomic force microscopy
LC	liquid crystal
LCD	liquid crystal display
MA	mercapto-allyl
n	index of refraction or LC director
PFPE	perfluoropolyether
PI	polyimide
POM	polarized optical microscopy
PRINT	pattern replication in non-wetting template
PU	polyurethane

1. Significance and History of Liquid Crystals and Liquid Crystal Displays

1.1. Introduction

1.1.1. Significance of LCDs

The invention of the liquid crystal display (LCD) has had significant impact on the ability of mankind to communicate. The relatively thin display has made cell phones, digital watches, digital music players, and laptop computers possible. With annual revenues of approximately $75 billion dollars for LCD TVs in 2008 they have become the dominant format for large screen displays.[1] At the heart of the LCD is a unique class of materials known as liquid crystals.

1.1.2. History of Liquid Crystals

In 1888 Friedrich Reinitzer was studying cholesteryl benzoate when he observed that upon heating it melted into a cloudy liquid at 145.5°C and into a clear liquid at 178.5°. He started a collaboration with Otto Lehmann and von Zepharovich which yielded three observations about the cholesterol: it had two melting points, it reflected circularly polarized light, and it rotated the polarization direction of light. Lehmann continued studying this new phase of matter using polarized optical microscopy and a heated stage. [2] Research in the field was slow, as most considered the new state of matter of little interest, until the1960s when optical displays using liquid crystals began to be fabricated. This new application led to increased research and the synthesis of stable, room temperature nematic liquid crystals that laid the foundation of a new industry. In order to understand how this

class of materials functions in electro-optical devices it is necessary to examine their physical and chemical properties.

1.2. Physical Properties of LCs

Varying degrees of microscopic order underlie differences in the material world around us. This is especially true for states of matter. Crystalline solids have orientational and positional order in three dimensions whereas liquid molecules tumble and flow randomly showing no signs of order, i.e. liquids are isotropic. There is another state of matter which flows like a liquid, but also possesses orientational and positional order called the liquid crystal phase. Liquid crystals are anisotropic.[3] If a substance possesses a liquid crystalline phase, it will be observed upon heating and occur between the crystalline and isotropic liquid phases as shown in Figure 1.1. The simplest liquid crystalline materials, termed nematic liquid crystals, exhibit one degree of orientational order but no positional order. The order found in this phase of matter is derived from the anisotropic intermolecular interactions in the fluid which in turn derive from the nature of the chemical structure of these small organic molecules. The chemical structure of a common nematic liquid crystal, called 5CB, is shown in Figure 1.2. The biphenyl group gives the liquid crystal an anisotropic, rod-like shape and steric interactions between biphenyl groups of different molecules drive the one degree of orientational order and a corresponding "director" **n**, an apolar vector specifying the unique optical axis of the nematic. The hydrocarbon tail disorders at the solid-LC transition providing an increase in entropy to offset the low entropy associated with anisotropic packing of the biphenyl axed in the ordered liquid. The cyano end group and the polarizability of the biphenyl group contribute to the anisotropic nature of the polarizability, when measured along the long axis of the molecule versus the short axis. Hence the dielectric

susceptibility is anisotropic ($\varepsilon \parallel \mathbf{n}$ is not the same as $\varepsilon \perp \mathbf{n}$) which makes it possible to manipulate the liquid crystals with electric fields. The anisotropy of the dielectric constant derives from the molecular orientational ordering and that in turn is accompanied by a difference in the index of refraction when measured along the director n because of the difference in polarizability of the long axis versus the short axis of the partially aligned molecules.[3] This anisotropy in index of refraction is known as birefringence and is the basis of the optical effects observed in LCDs.

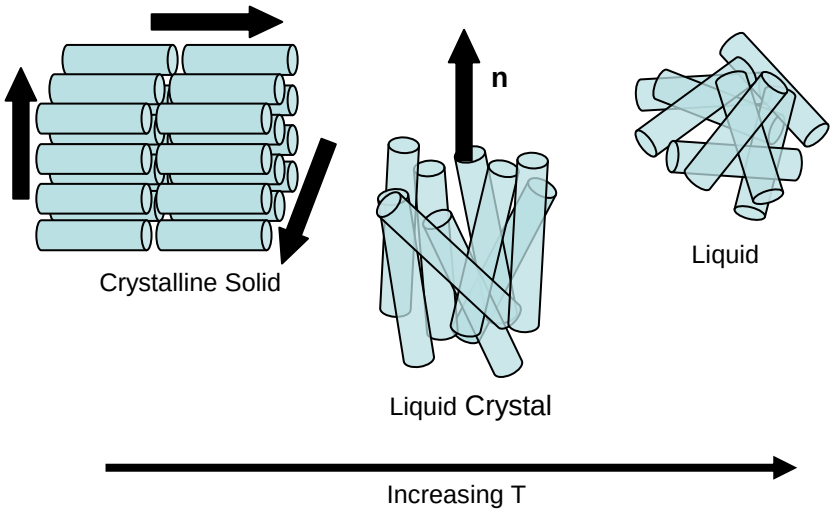

Figure 1.1 Temperature transition of crystalline solid to liquid crystal to liquid phase of matter as heat is added. The order in the liquid crystal phase is quite small compared to the crystalline solid based on the latent heat needed for a typical phase transition is ~250 J/g, while a typical liquid crystal to liquid phase transition requires ~ 5 J/g. The letter **n** represents the liquid crystal director or average orientation of the liquid crystal phase.

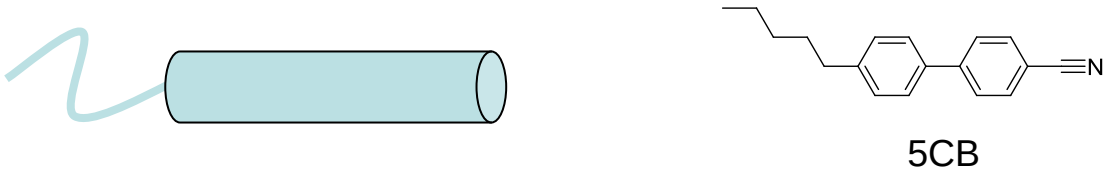

Figure 1.2 Schematic and chemical structure of the liquid crystal 5CB. The thermal and electro-optical properties of a liquid crystal are directly related to its chemical structure. The polarizability of biphenyl group and the dipole of the cyano group contribute to a difference in dielectric constant along the long axis of the molecule versus the short axis. This also leads to a difference in the index of refraction along the two axes.

1.3. Characterization of Liquid Crystals

1.3.1. Birefringence

Birefringence is defined as the division of light into two components (an ordinary, $\mathbf{n_0}$, and extraordinary, $\mathbf{n_e}$) found in materials which have two different indices of refraction in different directions (i.e., when light entering certain transparent materials, light splits into two beams which travel at different speeds). The quantity known as birefringence is defined as $\Delta\mathbf{n} = \mathbf{n_e} - \mathbf{n_o}$.[4] In liquid crystalline materials the extraordinary index of refraction is parallel to the director n, the average direction of the long axis of the molecule, the ordinary axis is perpendicular, and the birefringence can be related to the thickness of the liquid crystal phase by the equation:

$$\Delta n = n_{II} - n_{\perp} = \Gamma / t \qquad \text{eq. [1.1]}$$

In equation 1.1 Γ is the retardation of light and *t* is the thickness of the liquid crystal film.[3] The birefringence of liquid crystals makes it possible to observe the orientation of the director by polarized optical microscopy.

1.3.2. Polarized Optical Microscopy

When linearly polarized light enters a birefringent material parallel to one of the indexes of refraction, the light remains linearly polarized when it exits the material; however if it enters at an angle with respect to the principal indexes, elliptically polarized light exits the material, as shown in Figure 1.3. By employing linear polarizers before and after a LC sample, we can use this behavior to determine the orientation of the director of the LC. A schematic of the microscope setup is shown in Figure 1.4. The polarizer is placed in between

the light source and the sample. The analyzer is above the sample and the microscope objective. Both polarizer and analyzer can be rotated, but their polarizations are typically oriented perpendicular to one another in order to determine the orientation of the liquid crystal director. In this configuration, when the liquid crystal director is oriented in the same plane and parallel to either the polarizer or the analyzer, the light is extinguished and a dark state is observed. This occurs because the light retains its linear polarization and orientation such that when it exits the LC and hits the analyzer the polarization of the light and the analyzer are orthogonal. When the liquid crystal director is at an angle to either the polarizer or the analyzer, then the light is not extinguished, due to the formation of elliptically polarized light, and a bright state is observed. The intensity of light observed while rotating the liquid crystal director is described by the equation:

$$I_R = A^2 \sin^2 2\theta \sin^2\left[(\pi t / \lambda)(\Delta n)\right] \qquad \text{eq. [1.2]}$$

In eq. [1.2] A is the amplitude of the light wave, θ is the sample rotation with respect to the crossed polarizers, t is the sample thickness, λ is the wavelength of light, and $\Delta\mathbf{n}$ is the birefringence of the liquid crystal for the given wavelength of light.[3] As the initial LC director rotates with respect to the static polarizers, the orientation of the major axis of the elliptical light rotates giving rise to the observed change in intensity. If the liquid crystal director rotates between the bottom and top substrates, the angle of rotation can be measure by aligning the liquid crystal director on the bottom substrate parallel (or perpendicular) to the polarizer and rotating the analyzer until a dark state is observed. When a film of LC is deposited on a substrate, the LC director can orient in any number of directions. Therefore

one major and technologically important focus of LC research is the fabrication of substrates which induce uniform director alignment.

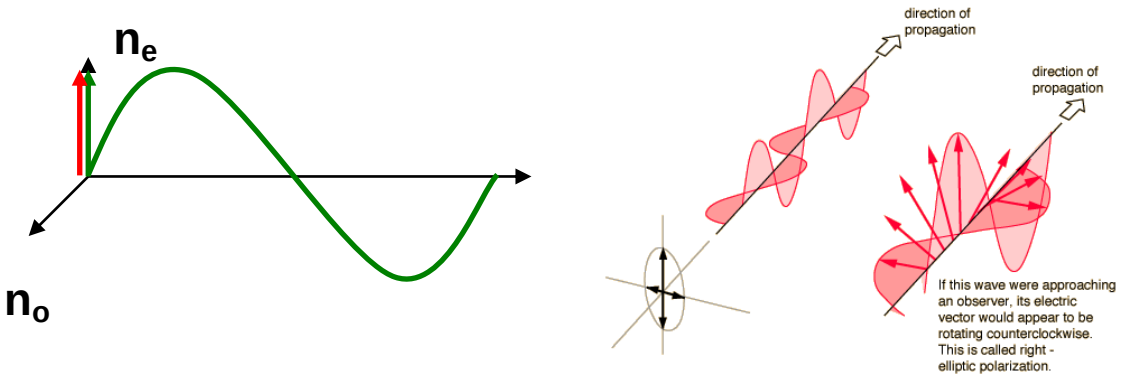

Figure 1.3 Effect of birefringent material on linearly polarized light.
Left: When linearly polarized light passes through a birefringent material, such as LCs, if the incident plane is parallel to ne or no, then no phase retardation occurs since the light interacts with only one index of refraction.
Right: If however, the incident plane is at an angle with respect to the two indexes of refraction the plane of light can be projected as two vectors parallel to the two indexes of refraction. Since there is a difference in the speed at which light travels along the two axes, a shift in phase occurs and elliptically polarized light is generated.

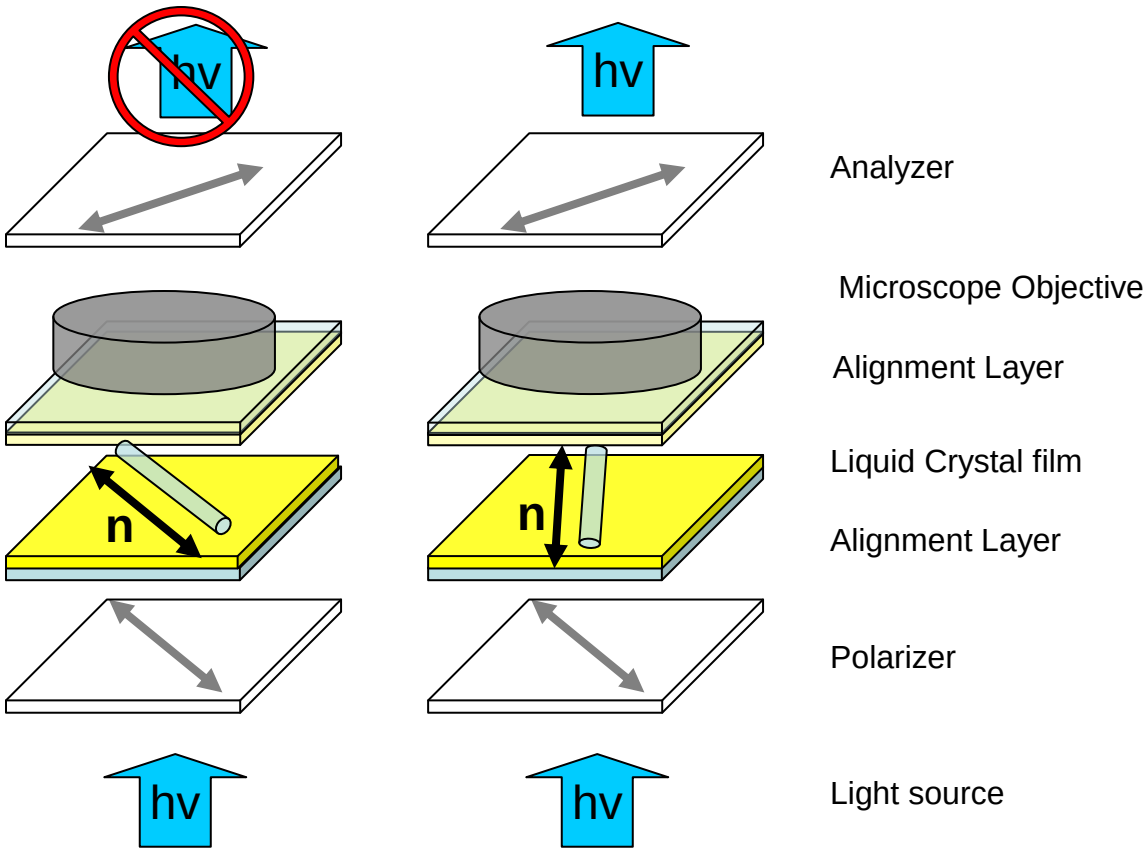

Figure 1.4 Schematic of Polarized Optical Microscopy setup. From bottom to top: light passes through a polarizer generating linearly polarized light. Alignment layers are used to manipulate the alignment of the liquid crystal director. Light then passes through the microscope objective which is located above the liquid crystal cell. A second polarizer, called the analyzer, is typically oriented perpendicular to the bottom polarizer. When the liquid crystal director is parallel to either the polarizer or the analyzer light is not able to pass and a dark state is observed. When the liquid crystal director deviates from being parallel to the polarizer or analyzer light is able to pass through and a bright state is observed.

1.4. LC Alignment

1.4.1. Terminology

When a liquid crystal comes in contact with a surface it chooses an alignment orientation in 3-D space based on the chemical and physical properties of the substrate. This phenomenon is known as "anchoring" of the director on a substrate—the selection of a specific orientation of n relative to the substrate surface. If the liquid crystal director is parallel to the plane of the surface it is termed planar alignment, see Figure 1.5. The angle between the long axis and the surface is termed the pre-tilt angle. The angle of rotation of the liquid crystal director with respect to a reference, such as a polarizer, is called the azimuthal orientation. Changes in light intensity are observed while rotating or changing the azimuthal orientation of a sample with planar alignment. Homeotropic alignment is achieved by increasing the pre-tilt angle to 90°, causing the liquid crystal director to be perpendicular to the substrate. Homeotropic alignment is evidenced by a "dark state" under crossed polars since the light propagates along the optical axis of the liquid crystal (**n**) and the birefringence of liquid crystal in this unique configuration is no longer able to retard the light passing through the sample.[3] At the heart of LC alignment and anchoring is the study of the chemical and physical mechanisms that determine how the LC and a substrate will interact.

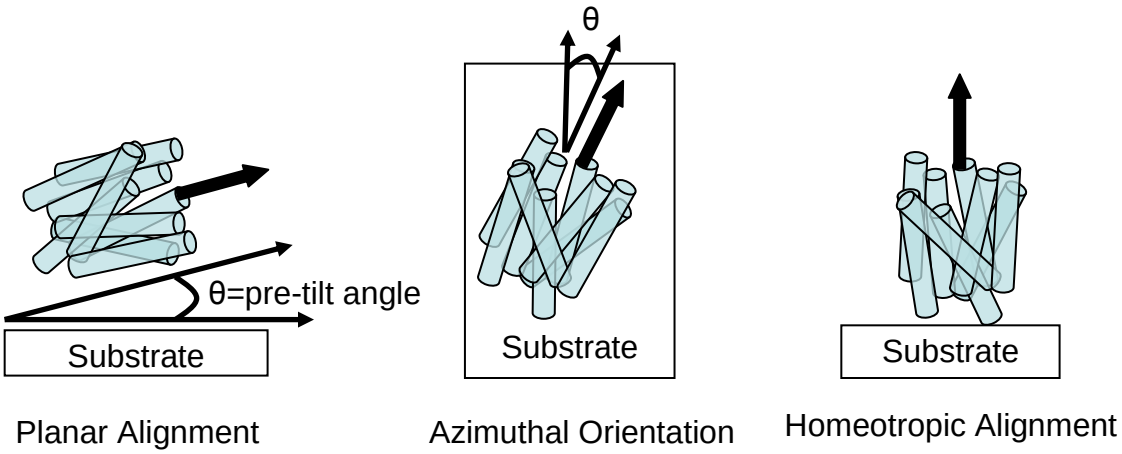

Figure 1.5 Schematic of different types of liquid crystal alignment, black arrow represents the LC director. Planar alignment occurs when the liquid crystal director is parallel to the substrate. Often there is a small angle between the substrate and the director; this is termed the pre-tilt angle. When viewed from above, the angle between the liquid crystal director and a reference line, such as a polarizer, is termed the azimuthal orientation. Homeotropic alignment occurs when the pre-tilt angle is 90°, i.e. the director is perpendicular to the substrate.

1.4.2. Mechanisms

Bulk liquid crystal alignment is similar to normal crystal growth in that there is a nucleation site from whence alignment/crystallization is propagated. For liquid crystals this occurs at the interface between the liquid crystal and a surface. Some materials exhibit weak anchoring interactions with the liquid crystal phase and multiple domains of different liquid crystal director orientation are observed. Other materials interact very strongly and induce uniform alignment over large areas and macroscopic distances from the substrate surface. These materials are most useful for electro-optical devices. Surfaces typically used to align liquid crystals are polymer films which have been mechanically rubbed[5-9], patterned[10, 11, 11, 12, 12-21], or fabricated with polarized light to align polymer chains without changing surface topography[22]. Alignment between the surface and the liquid crystals is driven by two possible mechanisms 1) the physical topography[5, 6, 16] of the surface and/or 2) the chemical interactions[3, 7, 23] between the liquid crystals and the aligned chemical moieties of the polymer chains. These mechanisms will be discussed in more detail in Chapter 2. While the debate over the mechanism of LC director alignment on surfaces continue, industry utilized the large scale, uniform alignment observed on rubbed polyimide films to fabricate the first generation of LCDs.

1.5. LCDs

1.5.1. Anatomy of a device

LCDs are an electro-optical multi-layered device that utilizes liquid crystals susceptibility to electrical fields, and their ability to bend light, to act as an on-off switch for an electro-optical pixel. The cross section of a twisted nematic LCD is shown in Figure 1.6. TN-LCDs use a white light source that is on whenever the display is in operation. A polarizer

is used to gain linearly polarized light. A thin film transistor is used to generate an electric field perpendicular to the substrates. Two alignment layers are used to control the orientation of the liquid crystal director in the absence of an electrical field. The first alignment layer is parallel to the bottom polarizer. The second alignment layer is perpendicular to the previous alignment layer, and parallel to the top polarizer. This causes the liquid crystal director to twist 90° from the bottom to the top of the device. When no electric field is applied, the linearly polarized light is twisted by the liquid crystal film such that it passes through the second polarizer. When an electric field is applied between electrodes the liquid crystal director aligns homeotropically, is unable to retard the light, and no light passes through due to the crossed polarizers.[3] A second device architecture known as In Plane Switching is shown in Figure 1.7. For this architecture the liquid crystals remain in a planar orientation; however they are rotated from parallel to one of the crossed polarizers, the dark state, to 45° from both polarizers, the bright state. This is typically done with multiple electrodes to generate electric fields at the desired angles in order to control the liquid crystal director orientation. Another method to obtain the desired orientation is to use multi-stable alignment layers. These layers exhibit stable alignment along more than one planar orientation due to surface patterning. This allows electric fields to be pulsed to induce switching from one orientation to another, instead of being constantly used to maintain the orientation. This results in reduced energy requirements.[12, 13, 17, 24] In order to fabricate and study the next generation of alignment layers, it is necessary to control both the chemical and physical nature of the surface. In this work we have employed micro and nano-scale fabrication methods to accomplish this goal.

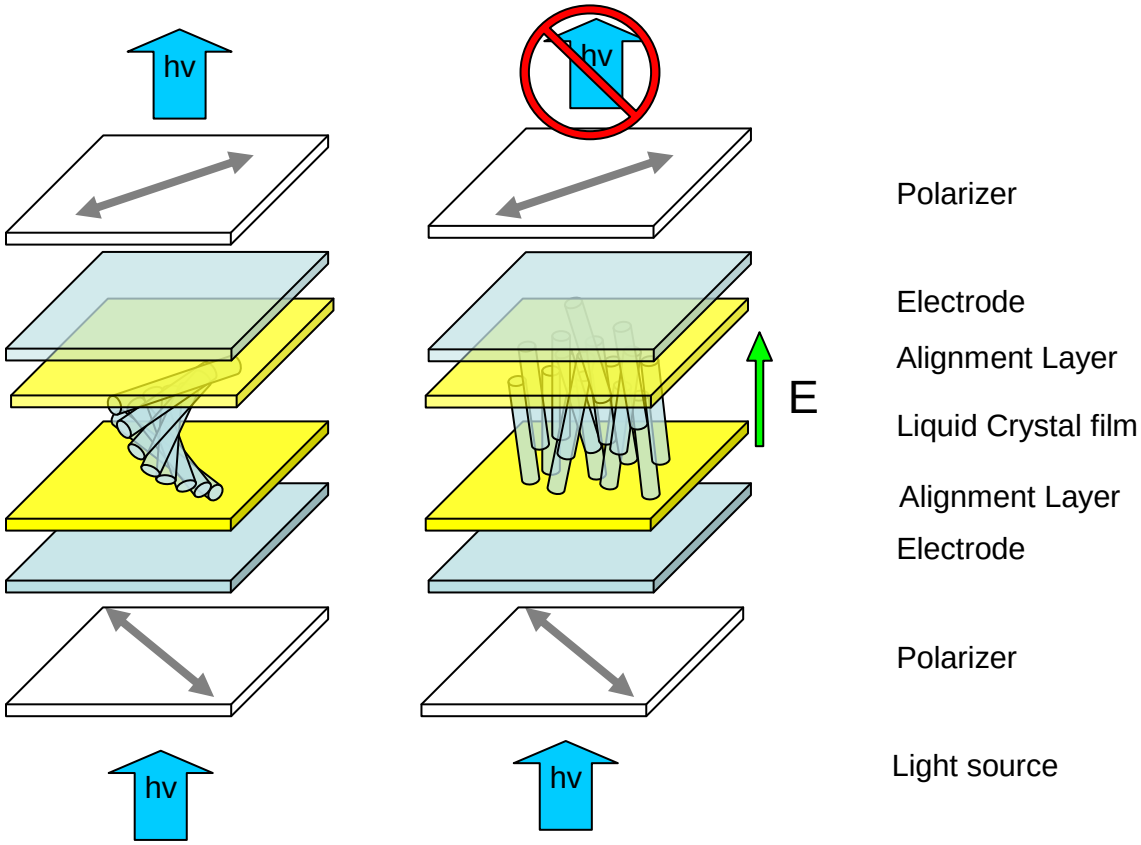

Figure 1.6 Schematic of a cross section of a twisted nematic LCD. The bottom alignment layer is oriented parallel to the bottom polarizer, grey arrows, and the top alignment layer is oriented to the top polarizer, called the analyzer. This causes the liquid crystals to twist 90° from bottom to top. When light is shown through the bottom polarizer the light is polarized parallel to the liquid crystal director at the bottom of the layer. As light progresses through the liquid crystal layer the twisting of the liquid crystal rotates the plane of polarization of the light allowing it to pass through the top polarizer, the pixel is bright. When an electric field is generated perpendicular to the plane of the substrate, the liquid crystal alignment becomes homeotropic and is not able to alter the polarization of the light and the top polarizer extinguishes the light, the pixel is dark.

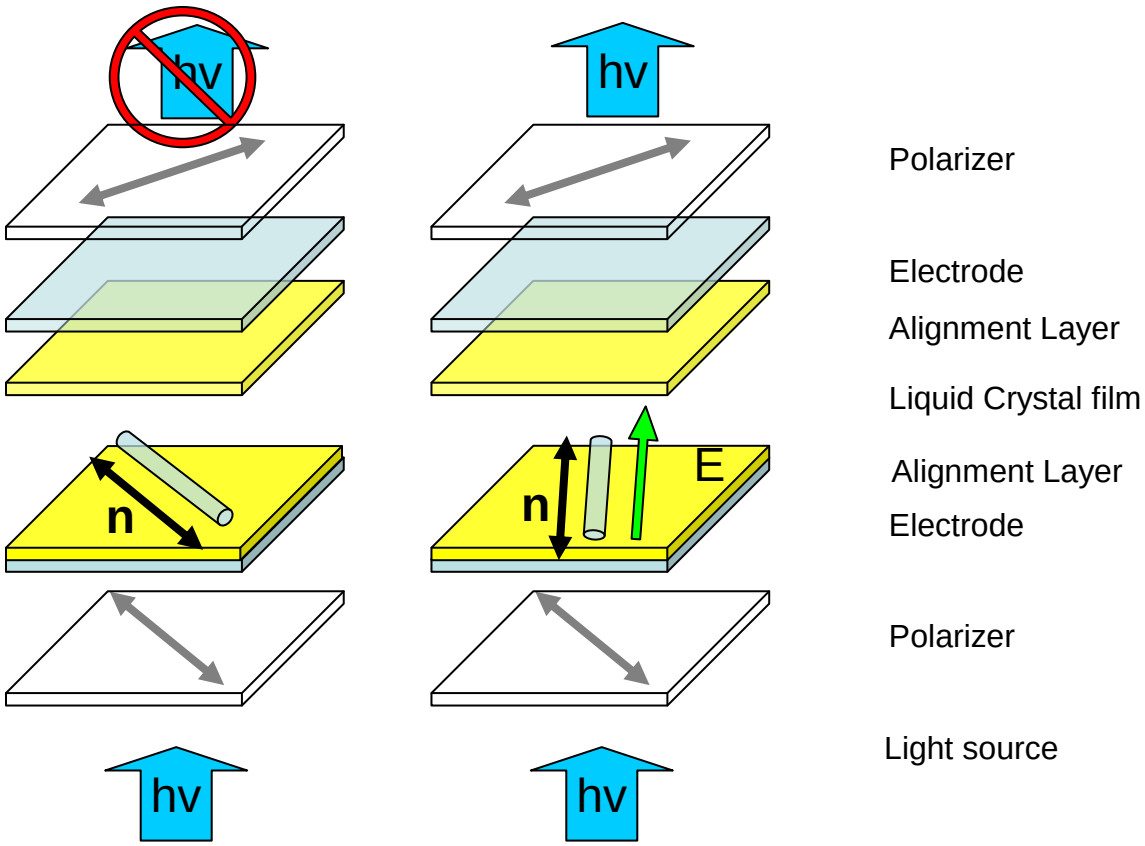

Figure 1.7 Schematic of a cross section of an IPS-LCD. No twisting occurs in this device. The dark state is achieved by making the orientation of the alignment layers parallel to each other and one of the polarizers. The bright state is achieved by generating an electric field parallel to the substrate, but at an angle of 45° with reference to the polarizers.

1.6. Nanoscale Patterning

The ability to make patterns on the nanoscale, 1nm-1μm, is useful for basic and applied research in many fields of science and engineering. The ability to fabricate and study materials on the nano-scale has led to the discovery of many interesting phenomenon[25-32] and devices[33-43]. One of the earliest methods for fabricating nano-scale patterns is photolithography. Patterns are generated by casting a photo sensitive polymer, called a photoresist, onto a substrate, exposing it with UV light that has passed through a patterned photomask to chemically alter specific areas of the photoresist, chemically developing and removing the unwanted areas of the photoresist, etching the pattern into the substrate, and removing the photoresist as shown in Figure 1.8. State of the art photolithography techniques can fabricate patterns with dimensions in the plane of the substrate on the order of 100nm, and heights as small as 10nm. It is the technique used by the semiconductor industry to fabricate the circuitry used in modern electronics. It is also the first step in newer methods of pattern generation such as nano-imprint lithography, NIL[44-46] and soft lithography[47-49]. In NIL a pattern that was fabricated by traditional photolithography methods on a hard template, such as silicon wafers or glass, is used to directly emboss soft materials, such as polymers, by bringing the template into direct contact with a precursor material that is typically photo-cured with UV light. In soft lithography, a UV or thermally curable prepolymer is cast onto a hard master made by traditional photolithography, cured into a cross-linked elastomer, and removed to fabricate a mold that is a negative of the original pattern. The mold is then used to transfer an ink, in the case of micro contact printing and nano transfer printing, or may be used to make a replica of the master template by molding a liquid prepolymer that is cured with UV light or heat.

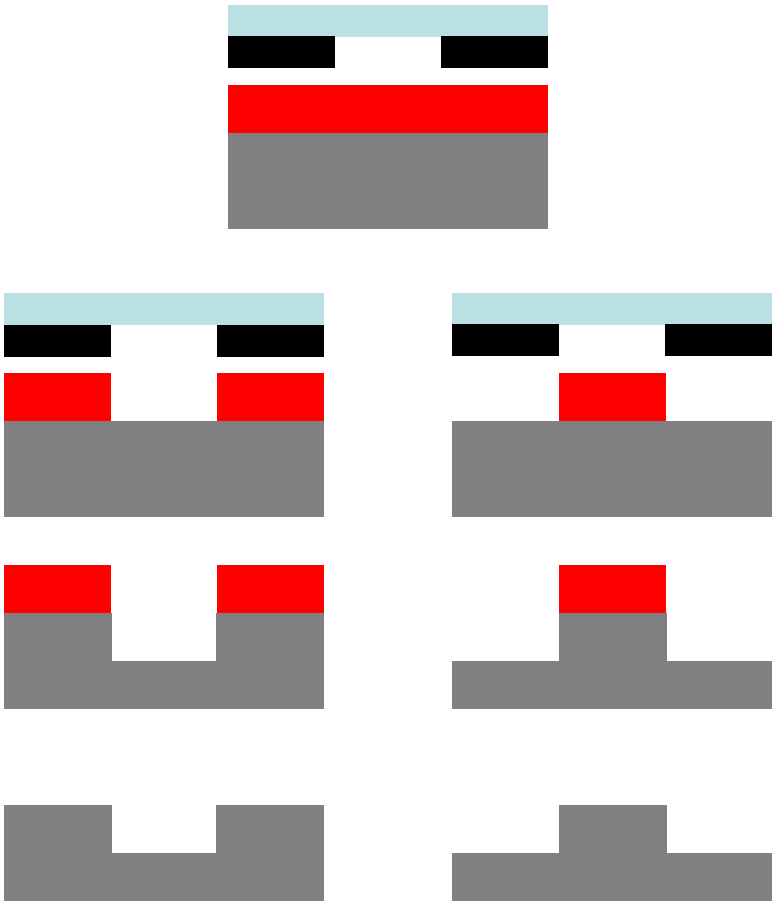

Figure 1.8 Schematic of the photolithography process. A photosensitive material is exposed with light that is passed through a patterned mask. Depending on the nature of the material the area exposed to light either stays or is removed. The pattern is then etched into the substrate and the photosensitive material is removed.

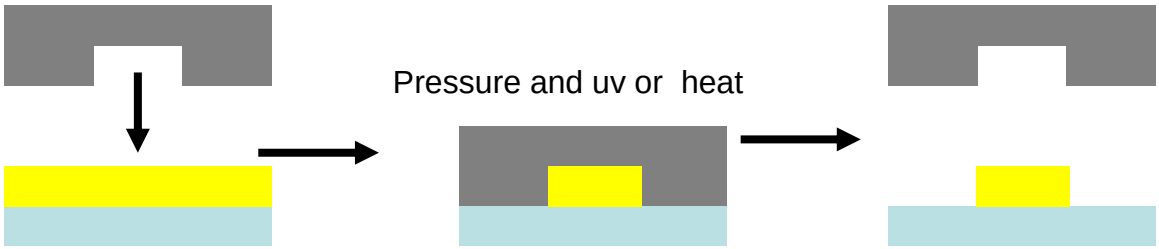

Figure 1.9 Schematic of the nano imprint lithography (NIL) method for fabricating nano-patterned uv curable materials. The grey template is typically fabricated by photolithographic methods as shown in figure 1.7. A uv curable material is cast onto a substrate and exposed to UV light while under physical pressure from the template. Upon removal of the template the nanopattern remains.

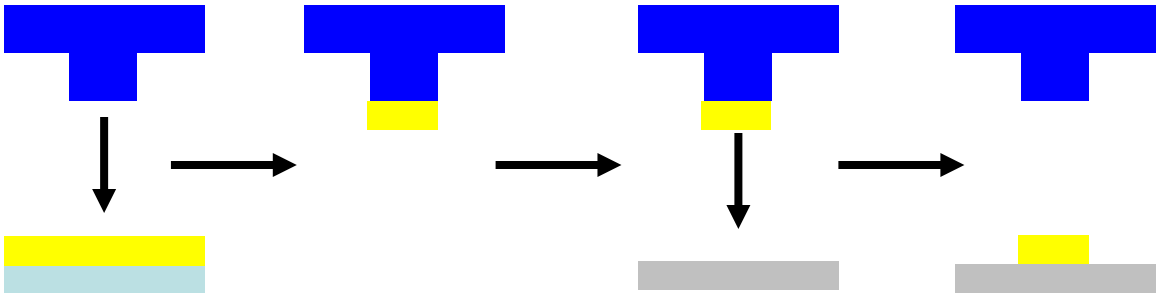

Figure 1.10 Schematic of nano transfer printing. A thermally or uv curable elastomer is used to mold the template. The mold is then brought into contact with an ink which can be a polymer solution, alkyl silanes, alkyl thiols, or any desired liquid formulation that will physically absorb onto the surface of the stamp and then be transferred to a new surface as illlustrated.

1.7. Research Objectives

Two main goals motivated this research. First, we wanted to understand the mechanism of liquid crystal alignment on the prototypical alignment layer of rubbed polyimide in order to use that knowledge to develop a new alignment layer fabrication method that is more conducive to a clean room environment, i.e. avoid the mechanical rubbing step. Second, we wanted to study the effect of complicated surface patterns on liquid crystal alignment in order to develop multi-stable and planar degenerate alignment layers. Chapter two discusses soft lithography as a tool for determining the mechanism of liquid crystal alignment on rubbed polyimide by embossing polymer films with line grating structures similar to those found on the surface of rubbed polyimide. We found that the interactions between the mold and the embossed polymer film have significant influence over liquid crystal alignment in the finished device. Chapter three discusses the effect of triangles in a hexagonal array, squares and rectangles in a square array, and Penrose tiling surface patterns on liquid crystal alignment. By frustrating the liquid crystal alignment with these patterns we found that we could make multi-stable devices and planar degenerate alignment layers.

Chapter four describes the microfabrication techniques used to fabricate the patterned silicon masters and inter-digitated electrodes used in the LC devices in the previous chapters. Chapter five is based on an earlier project where we employed nanoparticles synthesized in our lab into polymer based photovoltaics. We wanted to examine the relationship between aspect ratio of the nanoparticles and device performance, but found the size of the nanoparticles to inhibit the fabrication of properly working devices.

References

(1) Anonymous
DisplaySearch Revises Worldwide TV Forecasts; LCD TV Revenue Expected to Fall Y/Y for the First Time in LCD TV History.
http://www.displaysearch.com/cps/rde/xchg/displaysearch/hs.xsl/LCD_TV_Revenue_Expected_to_Fall_YY_for_the_1st_Time.asp.

(2) Anonymous
History and Properties of Liquid Crystals.
http://nobelprize.org/educational_games/physics/liquid_crystals/history/.

(3) Collings, P. J., 1947- In *Introduction to liquid crystals chemistry and physics;* Hird, M., Ed.; Taylor & Francis: London, 1997; .

(4) Weisstein, E. Eric Weisstein's World of Physics.
http://scienceworld.wolfram.com/physics/Birefringence.html.

(5) Berreman, D. W. *Molecular Crystals and Liquid Crystals* **1973**, *23*, 215.

(6) Berreman, D. W. *Phys. Rev. Lett.* **1972**, *28*, 1683-1686.

(7) Geary, J. M.; Goodby, J. W.; Kmetz, A. R.; Patel, J. S. *J. Appl. Phys.* **1987**, *62*, 4100-4108.

(8) Lee, E. S.; Vetter, P.; Miyashita, T.; Uchida, T. *Jpn. J. Appl. Phys.* **1993**, *32*, L1339.

(9) Lee, S. W.; Chae, B.; Kim, H. C.; Lee, B.; Choi, W.; Kim, S. B.; Chang, T.; Ree, M. *Langmuir* **2003**, *19*, 8735-8743.

(10) Chiou, D. -.; Chen, L. -.; Lee, C. -. *Langmuir* **2006**, *22*, 9403-9408.

(11) Gwag, J. S.; Oh-e, M.; Yoneya, M.; Yokoyama, H.; Satou, H.; Itami, S. *J. Appl. Phys.* **2007**, *102*, 063501.

(12) Yi, Y. W.; Khire, V.; Bowman, C. N.; Maclennan, J. E.; Clark, N. A. *J. Appl. Phys.* **2008**, *103*, 093518.

(13) Gwag, J. S.; Kim, J.; Yoneya, M.; Yokoyama, H. *Appl. Phys. Lett.* **2008**, *92*, 153110.

(14) Hah, H.; Sung, S.; Han, M.; Lee, S.; Park, J. *Materials Science and Engineering: C* **2007**, *27*, 798-801.

(15) Lee, B.; Clark, N. A. *Science* **2001**, *291*, 2576.

(16) Lin, R.; Rogers, J. A. *Nano Letters* **2007**, *7*, 1613-1621.

(17) Niitsuma, J.; Yoneya, M.; Yokoyama, H. *Appl. Phys. Lett.* **2008**, *92*, 241120.

(18) Rastegar, A.; Skarabot, M.; Blij, B.; Rasing, T. *J. Appl. Phys.* **2001**, *89*, 960-964.

(19) Ruetschi, M.; Grutter, P.; Funfschilling, J.; Guntherodt, H. -. *Science* **1994**, *265*, 512-514.

(20) S. Park, C. Padeste, H. Schift, J. Gobrecht,T.Scharf, *Adv Mater* **2005**, *17*, 1398-1401.

(21) Yi, Y.; Nakata, M.; Martin, A. R.; Clark, N. A. *Appl. Phys. Lett.* **2007**, *90*, 163510.

(22) Schadt, M. *Molecular Crystals and Liquid Crystals Science and Technology.Section A.Molecular Crystals and Liquid Crystals* **2001**, *364*, 151.

(23) Castellano, J. A. *Molecular Crystals and Liquid Crystals* **1983**, *94*, 33.

(24) Fukuda, J.; Gwag, J. S.; Yoneya, M.; Yokoyama, H. *Phys. Rev. E* **2008**, *77*, 011702.

(25) Kastner, M. A. *Phys Today* **1993**, *46*, 24.

(26) Reed, M. A. *Sci. Am.* **1993**, *268*, 118-123.

(27) Vijayakrishnan, V.; Chainani, A.; Sarma, D. D.; Rao, C. N. R. *J. Phys. Chem.* **1992**, *96*, 8679-8682.

(28) Likharev, K. K. *IBM J. Res. Dev.* **1988**, *32*, 144-158.

(29) Betzig, E.; Trautman, J. K. *Science (Washington, D. C. , 1883-)* **1992**, *257*, 189-195.

(30) Girard, C.; Dereux, A. *Rep. Prog. Phys.* **1996**, *59*, 657-699.

(31) Joannopoulos, J. D.; Villeneuve, P. R.; Fan, S. *Nature (London)* **1997**, *386*, 143-149.

(32) Talley, C. E.; Jackson, J. B.; Oubre, C.; Grady, N. K.; Hollars, C. W.; Lane, S. M.; Huser, T. R.; Nordlander, P.; Halas, N. J. *Nano Lett.* **2005**, *5*, 1569-1574.

(33) Bachtold, A.; Hadley, P.; Nakanishi, T.; Dekker, C. *Science (Washington, DC, U. S.)* **2001**, *294*, 1317-1320.

(34) Heo, Y. W.; Tien, L. C.; Kwon, Y.; Norton, D. P.; Pearton, S. J.; Kang, B. S.; Ren, F. *Appl. Phys. Lett.* **2004**, *85*, 2274-2276.

(35) Martel, R.; Schmidt, T.; Shea, H. R.; Hertel, T.; Avouris, P. *Appl. Phys. Lett.* **1998**, *73*, 2447-2449.

(36) Taminiau, T. H.; Stefani, F. D.; Segerink, F. B.; Van Hulst, N. F. *Nat. Photonics* **2008**, *2*, 234-237.

(37) Aryal, M.; Trivedi, K.; Hu, W. W. *ACS Nano* **2009**, *3*, 3085-3090.

(38) Craighead, H. G. *Science (Washington, D. C.)* **2000**, *290*, 1532-1535.

(39) Wang, Y.; Cao, G. *Adv. Mater. (Weinheim, Ger.)* **2008**, *20*, 2251-2269.

(40) Fafard, S.; Hinzer, K.; Raymond, S.; Dion, M.; McCaffrey, J.; Feng, Y.; Chabonneau, S. *Science (Washington, D. C.)* **1996**, *274*, 1350-1353.

(41) Senesi, A. J.; Rozkiewicz, D. I.; Reinhoudt, D. N.; Mirkin, C. A. *ACS Nano* **2009**, *3*, 2394-2402.

(42) Rolland, J. P.; Maynor, B. W.; Euliss, L. E.; Exner, A. E.; Denison, G. M.; DeSimone, J. M. *J. Am. Chem. Soc.* **2005**, *127*, 10096-10100.

(43) Ewing, A. G.; Strein, T. G.; Lau, Y. Y. *Acc. Chem. Res.* **1992**, *25*, 440-447.

(44) Chou, S. Y.; Krauss, P. R.; Renstrom, P. J. *J. Vac. Sci. Technol. , B* **1996**, *14*, 4129-4133.

(45) Chou, S. Y.; Krauss, P. R.; Renstrom, P. J. *J. Vac. Sci. Technol. , B* **1996**, *14*, 4129-4133.

(46) Chou, S. Y.; Krauss, P. R.; Renstrom, P. J. *Science (Washington, D. C.)* **1996**, *272*, 85-87.

(47) Xia, Y.; Whitesides, G. M. *Annu. Rev. Mater. Sci.* **1998**, *28*, 153-184.

(48) Xia, Y.; Whitesides, G. M. *Angew. Chem. , Int. Ed.* **1998**, *37*, 550-575.

(49) Gates, B. D.; Xu, Q.; Love, J. C.; Wolfe, D. B.; Whitesides, G. M. *Annu. Rev. Mater. Res.* **2004**, *34*, 339-372.

2. LC Alignment on Polymer Line Gratings

2.1. Introduction

2.1.1. Rubbed PI: Topography versus Chemical Interactions

Liquid crystal alignment layers fabricated by soft lithography represent an appealing alternative to the current mechanical rubbing process for future device fabrication due to a possible reduction in defects and the ability to use more complex surface patterns. However, since liquid crystal alignment is very sensitive to the chemical properties of the surface, the interaction between the mold and embossed polymer during fabrication must be carefully studied. Soft lithography has been used as a method to examine the alignment mechanism of LCs on rubbed polyimide (PI). Berreman[1, 2] originally posited that rubbing resulted in mechanical scoring of the substrate, and the resulting corrugated topography aligned the LC director n in the low-elastic-energy configuration (**n** || corrugation grooves) and was dependent on the amplitude and wavelength of the topography according to the following equation.

$$w_B = \left(\frac{\pi^3 K}{2\lambda}\right)\left(\frac{2A}{\lambda}\right)^2 \qquad \text{Eq. [2.1]}$$

In equation [2.1], w_B is the surface anchoring energy, K is the elastic constant of the liquid crystal, λ is the wavelength of the surface topography, and A is the amplitude. This explanation of the origin of director alignment was somewhat verified by using soft lithography to emboss microscopic grooves in polyimide to align **n**[3]; varying the amplitude

of the embossed corrugation affects the LC alignment suggesting that the Berreman mechanism is operative. However, the amplitude of those embossed features was 10 to 100 times larger than those produced by the rubbing process calling into question the Berreman mechanism for rubbed PI. Rogers et al[4] successfully aligned LCs by molding rubbed PI with PDMS and embossing UV and thermally curable polymers such as polyurethane and SU-8. However, since they did not emboss PI, the industry standard for alignment layers, it is still unclear whether the Berreman mechanism exclusively applies in rubbed PI LC alignment cells.

Others disagreed with the Berreman elasticity based explanation of director alignment and claim liquid crystal alignment on rubbed PI is driven by chemical interactions between the liquid crystal and PI functional groups which in turn were aligned by the mechanical rubbing process. X-ray scattering[5, 6] and polarized infrared[7, 8] experiments have shown that rubbing does align the polymer chains suggesting that functional groups may exhibit preferential orientation and contribute to specific interactions with the LC. LC alignment layers have also been made by methods such as bulk cold-drawing [9], Langmuir-Blodgett, and photo-alignment[10, 11] that do not create any surface topography. These results suggest that alignment of the polyimide chains is sufficient to initiate LC alignment, but does not rule out contributions from the surface topography.

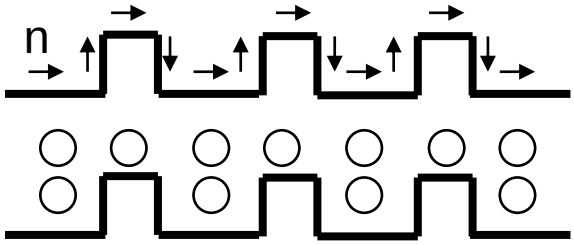

Figure 2.1 Schematic representation of LCs aligning perpendicular to (top) and parallel to (bottom) a line grating. **Top:** The arrows represent localized LC directors and illustrate how when perpendicular to the substrate the elastic tendency of the LCs to overlap in orientation would be distorted by the surface topography. **Bottom:** The circles represent LC directors perpendicular to the plane of the image and parallel to the line grating. The overlap of LC directors minimizes elastic strain. It would require significantly more energy to orient LCs perpendicular to the line gratings according to Berreman's hypothesis.

One of the problems with the fabrication method of mechanical rubbing is that physical contact between the felt roller and the polymer film is the main source of defects, i.e. dust and surface defects. It has also been observed that PDMS brought into physical contact with oligomeric cinnamate based photo-alignment layers can affect the pretilt angle upon removing the PDMS by peeling.[12] When developing a new fabrication method for LC alignment where physical contact with the alignment layer is involved, such as soft lithography, it is likely that the interaction between the mold and the alignment layer will have some effect of LC alignment. Herein we report the simultaneous existence of two LC alignment mechanisms in devices having embossed polymer line gratings and flat surfaces generated by soft lithography. The two alignment mechanisms are 1) alignment layer topography and 2) chemical surface modification during peel-off. The dominant mechanism is dependent on the line grating dimensions, the chemical properties of the alignment layer polymer, and the chemical properties of the mold.

2.2. Experimental Section

2.2.1. Materials and Instrumentation

Glass substrates were cleaned by sequential sonication in soapy water, acetone, and isopropanol for 10 minutes each, dried with nitrogen, and stored in an oven at 110°C. Silicon wafers were purchased from Silicon Quest. Flat Silicon wafers were cleaned with Piranha solution before molding. Polyimide precursor solutions were used as received. Pentaerythritol tetrakis(3-mercaptopropionate) and triallyl-1,3,5-triazine-2,4,6-(1H,3H,5H)-trione were purchased and used as received from Sigma-Aldrich,.Norland optical adhesive 73, polyurethane, was used as received. PFPE prepolymer formulation OMU-01, OMU-02, and OAE-01 from Liquidia Technologies, Inc. was used with added DEAP photoinitiator.

AFM images were measured with an Asylum MFP 3D, POM images were captured with an Olympus BX-61 polarized light setup.

2.2.2. Fabrication of Embossed polymer LC alignment devices via PRINT

Three PFPE prepolymer formulations were used for mold fabrication. All three have surface energy of ~15-20 dyne/cm, but OMU-02 has a modulus of 30 MPa compared to 8-10 MPa for OMU-01 and OAE-01. The chemical differences between the formulations are proprietary. Figure 2 schematically illustrates the soft lithography process PRINT[13] (Pattern Replication In Non-wetting Template) used to emboss polymer LC alignment films and the fabrication of the LC cells. Three types of masters were fabricated to serve as the template, line grating example shown in step A:

- First, silicon line gratings were fabricated using standard photolithographic techniques and reactive ion etching with chlorine plasma which are described in more detail in Chapter 4.
- Second, conventional rubbed PI films were fabricated by spin coating PI precursor solution onto cleaned glass slides, baking at 90°C for 30 minutes and 180°C for 30 min, and rubbing the PI-coated glass with a rotating felt roller at room temperature while the substrate was translated normal to the roller axis.
- Third, a cleaned silicon wafer was used as a master for flat polymer films. In step B and C, PFPE prepolymer was drop cast onto a template, cured under nitrogen with UV light for 3 minutes, and then peeled off of the template.

Polymer replicas were fabricated as shown in steps D and E by two different methods. First, PI films were made when PI precursor solution was spun coat onto cleaned

glass slides, the PFPE mold was placed on the wet film, pressure was applied, and the film was soft baked at 90°C (30 min) and hard baked at 180°C (30 min). Second, mercapto-allyl(MA) and polyurethane(PU) films were made by drop casting precursor formulations onto cleaned glass slides, the PFPE mold was placed on the wet film, and cured under nitrogen with UV light for 5 minutes. For all films, the molds were peeled at 45° relative to the line grating/rubbing direction as shown in steps F and G. The embossed films were characterized by tapping mode AFM. LC cells were fabricated by dispersing ~5μm diameter polymer bead spacers onto one of the embossed films and placing a second (embossed) film on top of the spacer-coated film such that the peeling direction of both films on the interior of the cell was parallel and shown in step G. The cells were heated to 90°C and the LC 5CB was added by capillary force in its isotropic state, and then cooled to room temperature when LC alignment spontaneously formed in the cell. LC alignment cells were characterized by polarized optical microscopy.

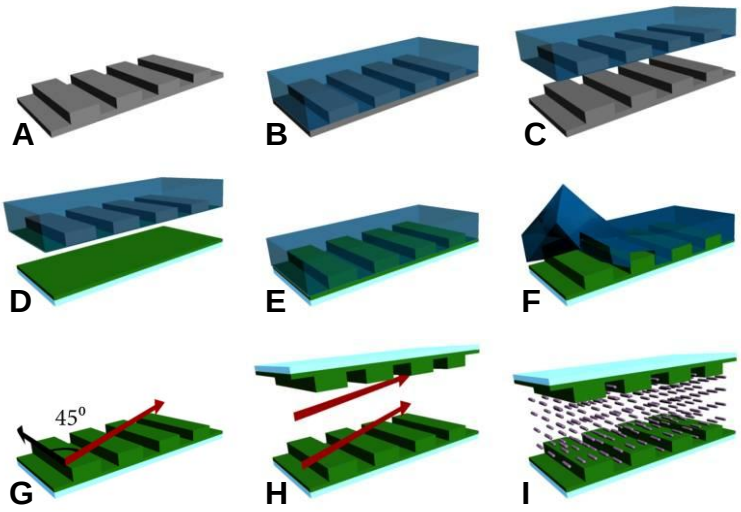

Figure 2.2 Schematic of the fabrication process for LC alignment cells. The master template is replicated by drop casting PFPE precursor and curing with UV light. The PFPE mold is then placed on a UV or thermally curable film and the mold is filled by capillary force. The mold is peeled off the cured polymer replica at a 45° angle with respect to the line grating; the red arrows represent the peeling direction. Two replicas are then aligned with line grating and peeling directions parallel and the cell is filled with LC by capillary force.

2.3. Results and Discussion

2.3.1. LC Alignment Dependence on the Chemical Nature of the Embossed Polymer

Figure 3 shows representative AFM height images of PU line gratings (AFM images of all line gratings are shown at the end of the chapter in figures 2.10-2.12). PU and MA exhibit very good fidelity to the line grating dimensions of the silicon master, but PI line gratings exhibit shrinkage in comparison due to the evaporation of solvent. During the fabrication of the alignment films, the molds were removed by peeling at 45° relative to the line grating direction in order to determine if this affected liquid crystal alignment. Figure 3 shows POM images of PI, MA, and PU line gratings, made with OMU-01 molds, taken with the line grating aligned parallel to the polarizer. Dark states indicate n is parallel to the line grating, while bright states indicate n is aligning, to some degree, with the peeling direction. PI alignment layers show alignment parallel to the peeling direction for all feature dimensions fabricated. For MA alignment layers the Berreman mechanism is evident in that the surface topography dominates for 95 nm deep grooves; however, as the depth of the embossed grooves is decreased, the alignment relative to the grating direction begins to deviate towards the peel-off direction. For 2 and 3 μm groove widths the transition appears to be gradual for all line heights, whereas the smaller groove widths have a sharp transition at a line height of 25nm. PU films show very little dependence on the peeling direction until a line height of 10nm, where the alignment depends strongly on the peeling direction. Assuming any alignment effects from peeling the mold from the surface are constant, the alignment trend agrees with Berreman's equation in that the strength of the alignment from the surface topography is proportional to the amplitude and disproportional to the wavelength. Clearly alignment is caused by the line gratings when the topographical features

are sufficiently deep while alignment caused by the peeling is secondary. However, it is important to note that the depth that is sufficient to overcome peeling varies depending on the polymer that is embossed indicating that the alignment strength of the peeling effect is material dependent.

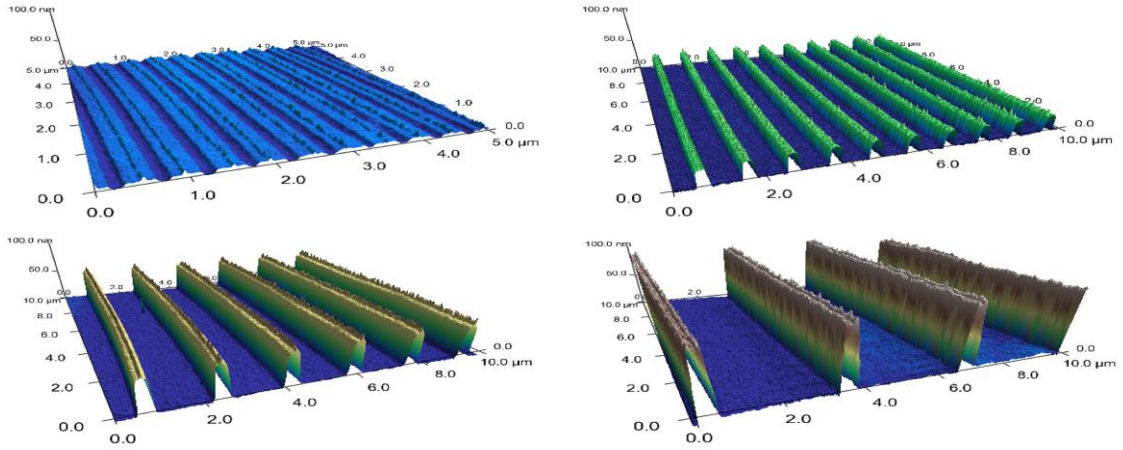

Figure 2.3 Representative AFM height images of PU line gratings fabricated by the PRINT soft lithography method. All line widths are 250nm. The lines in the top left image are 10nm tall and have 250nm wide grooves. The lines in the top right are 25nm tall and have 750nm wide grooves. The lines in the bottom left image are 50nm tall and have 1500nm wide grooves. The lines in the bottom right image are 95nm tall and have 3000nm wide grooves.

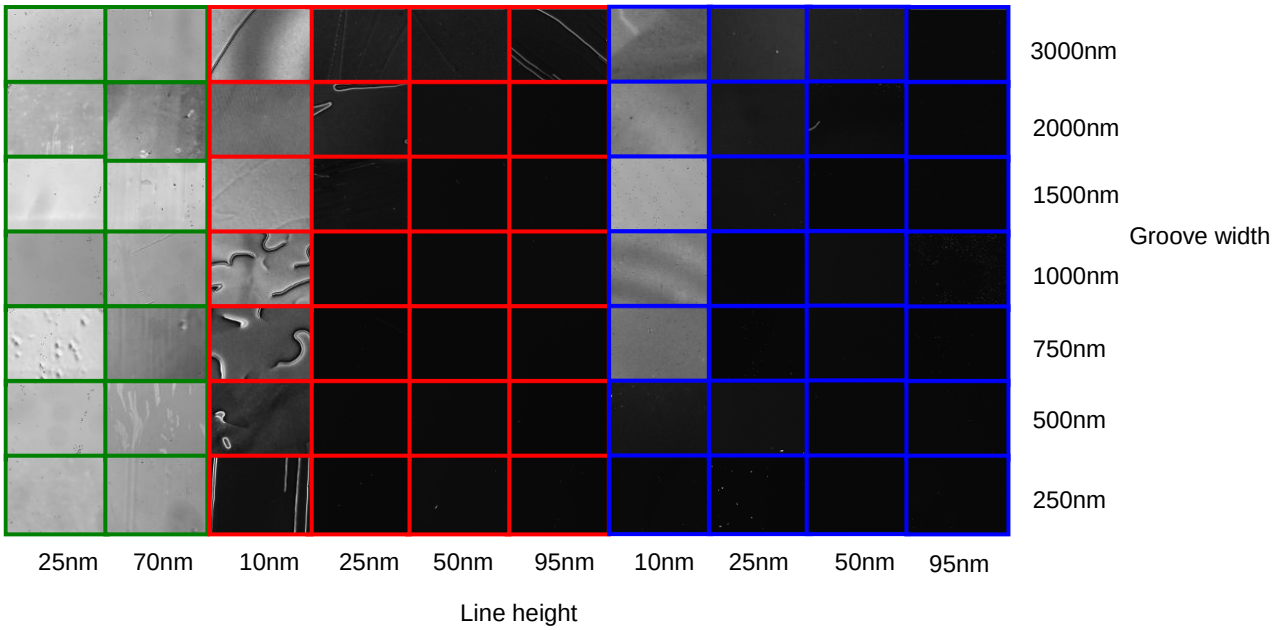

Figure 2.4 POM images of line grating replicas made from PI, MA, and PU outlined in green, red, and blue. The line gratings were aligned parallel to the polarizer. The bright states indicate the liquid crystal director alignment is being influenced by the peeling direction of the mold removal. The dark states indicate the line grating topography is controlling the alignment of the liquid crystal director. These results agree with Berreman's formula's prediction that liquid crystal alignment by surface topography is dependent on the amplitude and periodicity. It also illustrates sensitivity to surface interactions during fabrication are material dependent.

2.3.2. LC Alignment Dependence on the Chemical Nature of the Mold

To observe the effect of mold chemistry on LC alignment two additional PFPE formulations, OMU-02 and OAE-01, were used to fabricate line gratings with 500 and 2000 nm groove widths. POM images of line gratings aligned parallel to the polarizer is shown in Figure 4, the data for OMU-01 was taken from Figure 3. Even though there are only slight differences in surface energy and modulus between the PFPE formulations, it is significant enough to fabricate line gratings that show little or no dependence on the peeling direction for PU films. This gave evidence that it should be possible to replicate the topography of rubbed PI and observe LC alignment with no peeling effects.

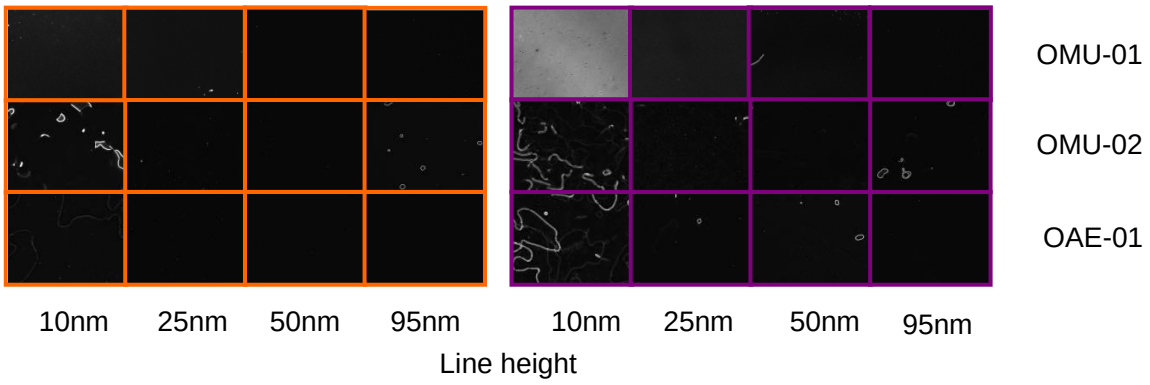

Figure 2.5 POM images of PU line grating replicas made from OMU-01, OMU-02, and OAE-01 molds. 500nm groove widths are outlined in orange and 2000nm groove widths are outline in purple. The images for OMU-01 are taken from Figure 3. Devices made using OMU02 and OAE-01 molds align with the line gratings as evidenced by the dark states. Only the 10 nm heights and 2000nm groove width gratings show a slight peeling effect as evidenced by the slightly lighter shade of black.

To verify further that the mold chemistry could affect the peeling effect on LC alignment, flat polymer films were fabricated and AFM height images are shown in Figure 6. PI films exhibit relatively large surface roughness values for all mold formulations, whereas MA and PU films exhibit relatively smooth films. We believe this may be caused by solvent evaporation during the baking process. Figure 6 shows POM images of LC devices with the peeling direction parallel to the polarizer. Devices made from OMU-01 show uniform LC alignment parallel to the peel direction for PI and MA; however PU films exhibit a fingerprint like texture. This reinforces our observations from the line grating topographies that OMU-01 has a strong peeling effect. We are unsure as to the cause of the interesting texture observed for the PU films. OMU-02 shows LC alignment parallel to the peel direction for PI, however MA and PU films exhibit a mixture of alignment domains. LC alignment in these devices seem to be more sensitive to surface defects, since most of the observed disclinations coincide with optically observable defects in the polymer film. OAE-01 shows a very fine random LC alignment texture for PI films, whereas MA and PU films show larger domains of random LC orientation with many defects. As observed with the line grating topographies OAE-01 seems to have the least peeling dependence.

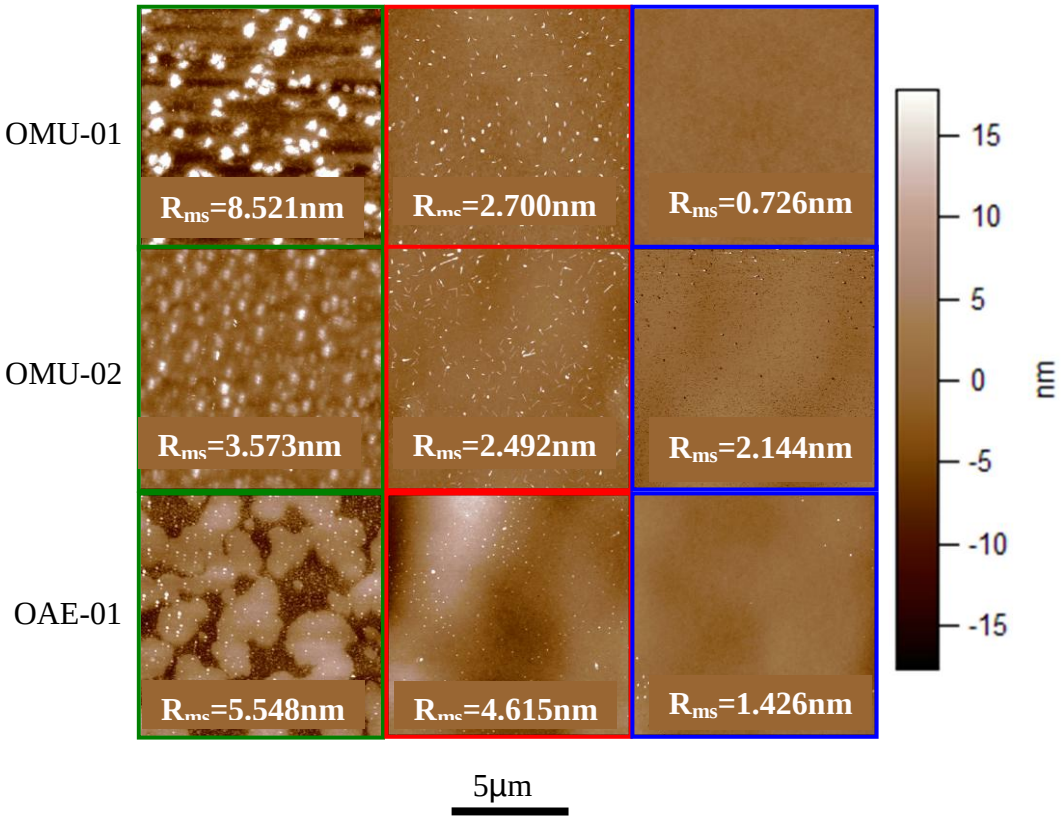

Figure 2.6 AFM height images of flat PI, MA, and PU replicas highlighted as green red, or blue. Insets are the surface roughness. PI films were quite rough most likely due to the evaporation of solvent during the curing process.

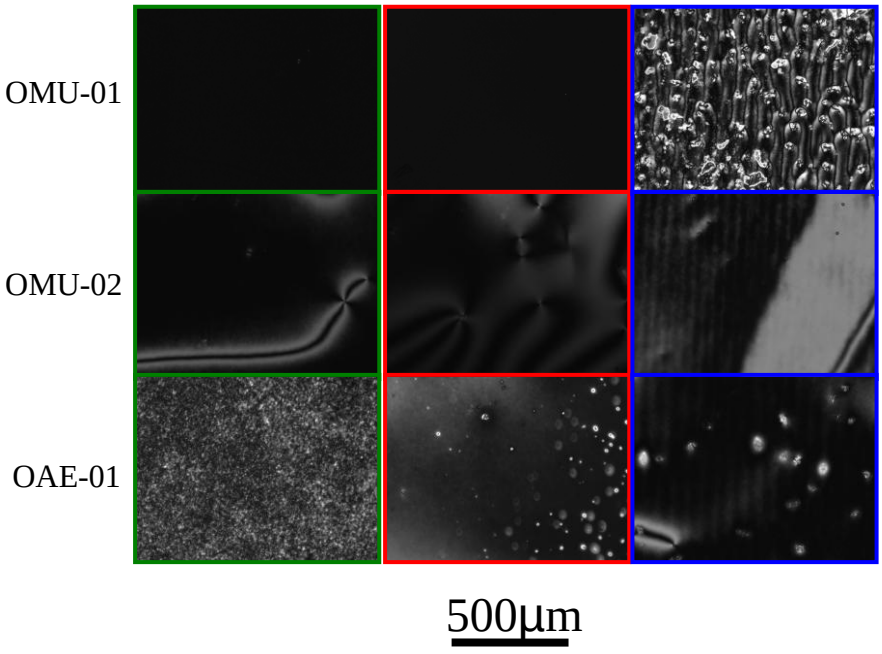

Figure 2.7 POM images of flat PI, MA, and PU replicas highlighted as green red, or blue. The peeling direction was aligned parallel to the polarizer. PI and MA films from OMU-01 and OMU-02 molds show significant alignment from the removal of the mold, the other films showed non-uniform alignment.

2.3.3. Rubbed PI Replica LC Alignment Layers

AFM height images, shown in Figure 7, of rubbed PI replicas show good fidelity for all MA and PU films, but the PI films tend to lose some of the smaller line features. This is most likely due to shrinkage from solvent evaporation as noted for the line grating alignment layers. POM of LC alignment devices shown in Figure 8 were taken with the rubbed line direction parallel to the polarizer. Devices made from OMU-01 show a bright state indicating dependence on peeling for PI, MA, and PU films. The PU films still exhibit the fingerprint texture seen in the flat devices. OMU-02 devices are a random mixture of domains indicating that in the dark domains the surface topography dominates while in the bright domains peeling removal of the mold is affecting the LC alignment. This suggests the alignment strength of the surface topography and the surface modification due to peeling is roughly equivalent, but is not uniform throughout the entire device. OAE-01 devices show a bright state for PI films, indicating peeling dependence, but a dark state is observed for MA and PU indicating the LC alignment is dictated by the surface topography. This shows that the topography observed on rubbed PI is sufficient to uniformly align LCs, however it also shows that it is quite sensitive to the materials used during fabrication by soft lithography.

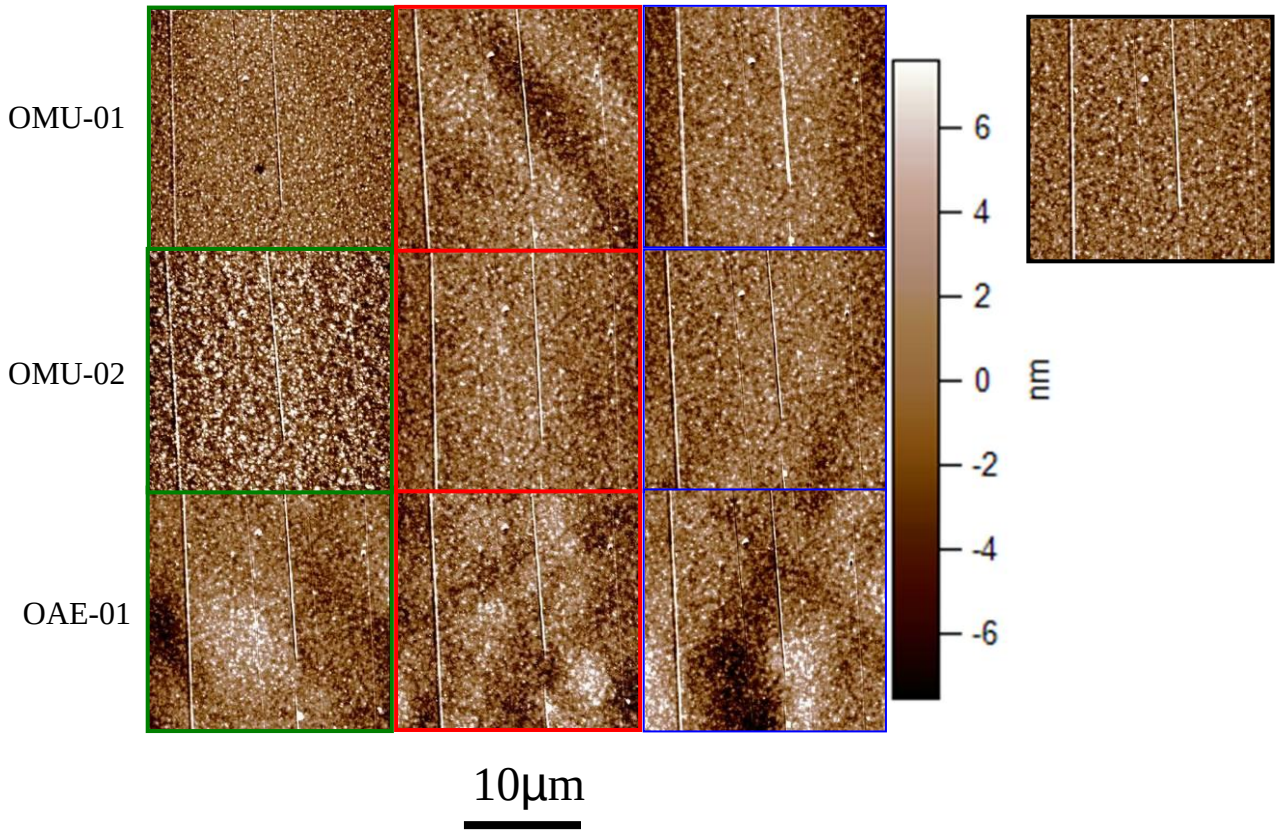

Figure 2.8 AFM height images of rubbed replicas made of PI, MA, and PU highlighted as green red, or blue and the template rubbed PI in black. All films show good fidelity to the surface topography observed in the template.

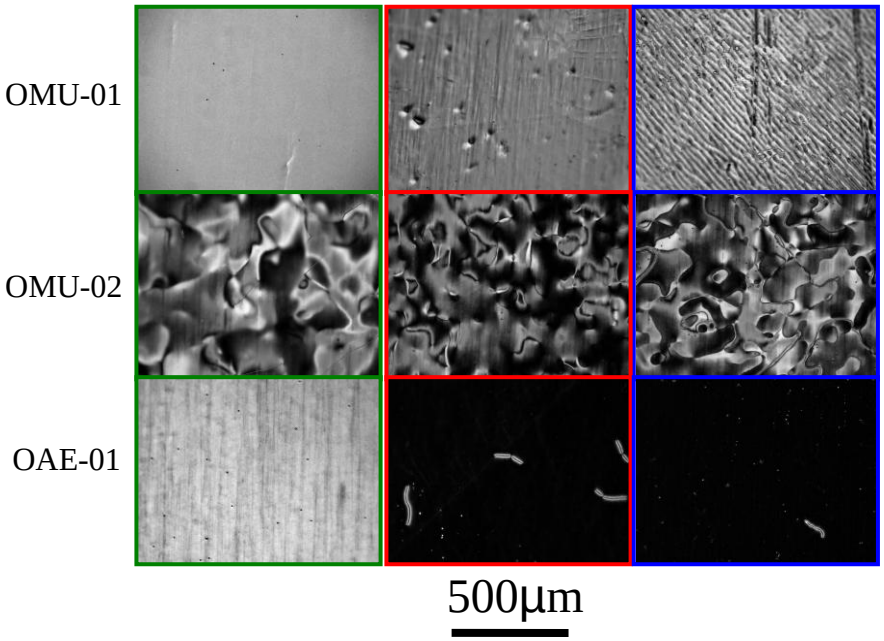

Figure 2.9 POM images of PI, MA, and PU replicas of rubbed PI highlighted as green red, or blue. The rubbed line direction was aligned parallel to the polarizer and the peeling direction at a 45° angle with respect to the polarizer. Bright states indicate alignment along the peeling direction and dark states indicate alignment along the rubbed line direction. All films made with OMU-01 molds show alignment along the peeling direction. All OMU-02 films show a mixture of domains that follow either the peeling or rubbed line direction. The PI film made from OAE-01 mold follows the peeling direction, but the MA and PU films follow the rubbed lines. This data illustrates that it is possible for the surface topography found on rubbed PI can align LCs, but it is sensitive to the interactions between the mold and the embossed film.

2.4. Conclusions

Berreman's hypothesis of surface topography being able to align LCs was supported by the results of our experiments; however, the sensitivity of LC alignment to surface modification by physical contact with and controlled removal of a mold during fabrication removal of the PFPE molds by peeling illustrates that chemical interactions between the LC and the alignment surface can align LCs as strongly as the line gratings. It is reasonable to conclude that in rubbed PI the surface topography and the aligned chemical functional groups of the PI work in concert to align LCs. Soft lithography is a good method for fabricating LC alignment layers, but care must be taken to use the right combination of alignment layer and mold to avoid any peeling effect or design the alignment layer in such a way that the two mechanisms can work in concert.

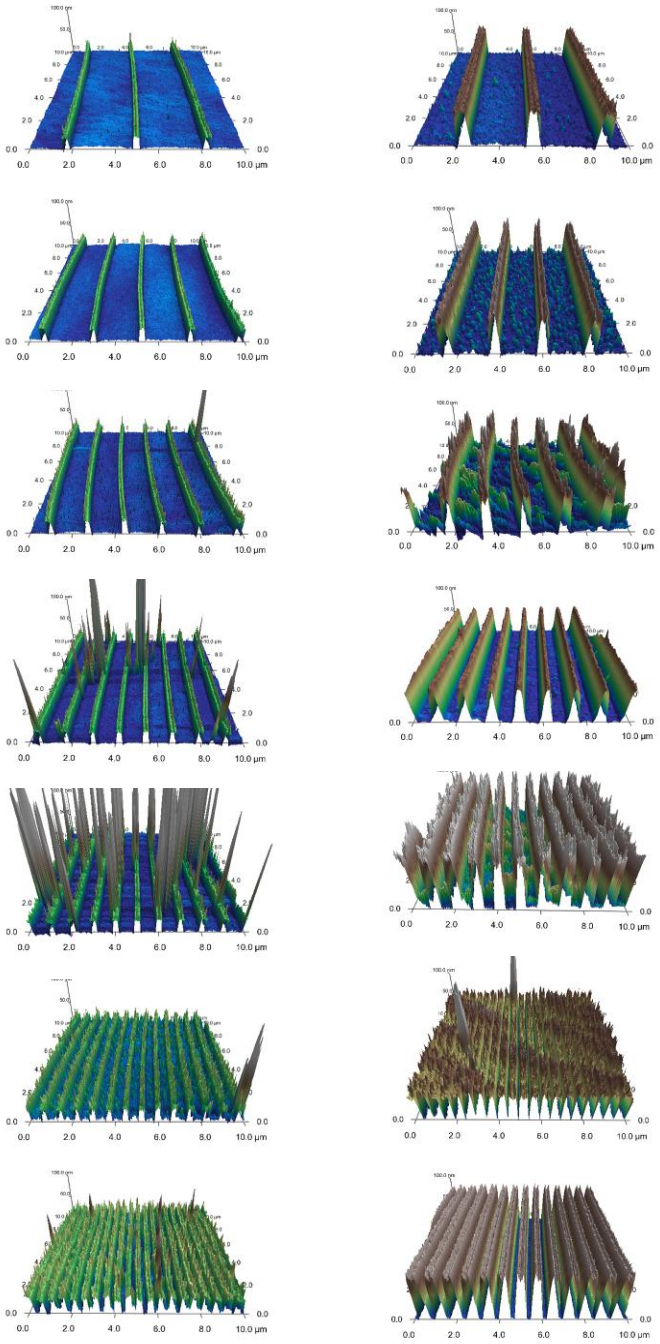

Figure 2.10 AFM height images of embossed PI line gratings. The line gratings in the left column are 25nm tall, and 70nm tall in the right column. The groove widths from top to bottom are 3μm, 2μm, 1.5μm, 1μm, 750nm, 500nm, and 250 nm.

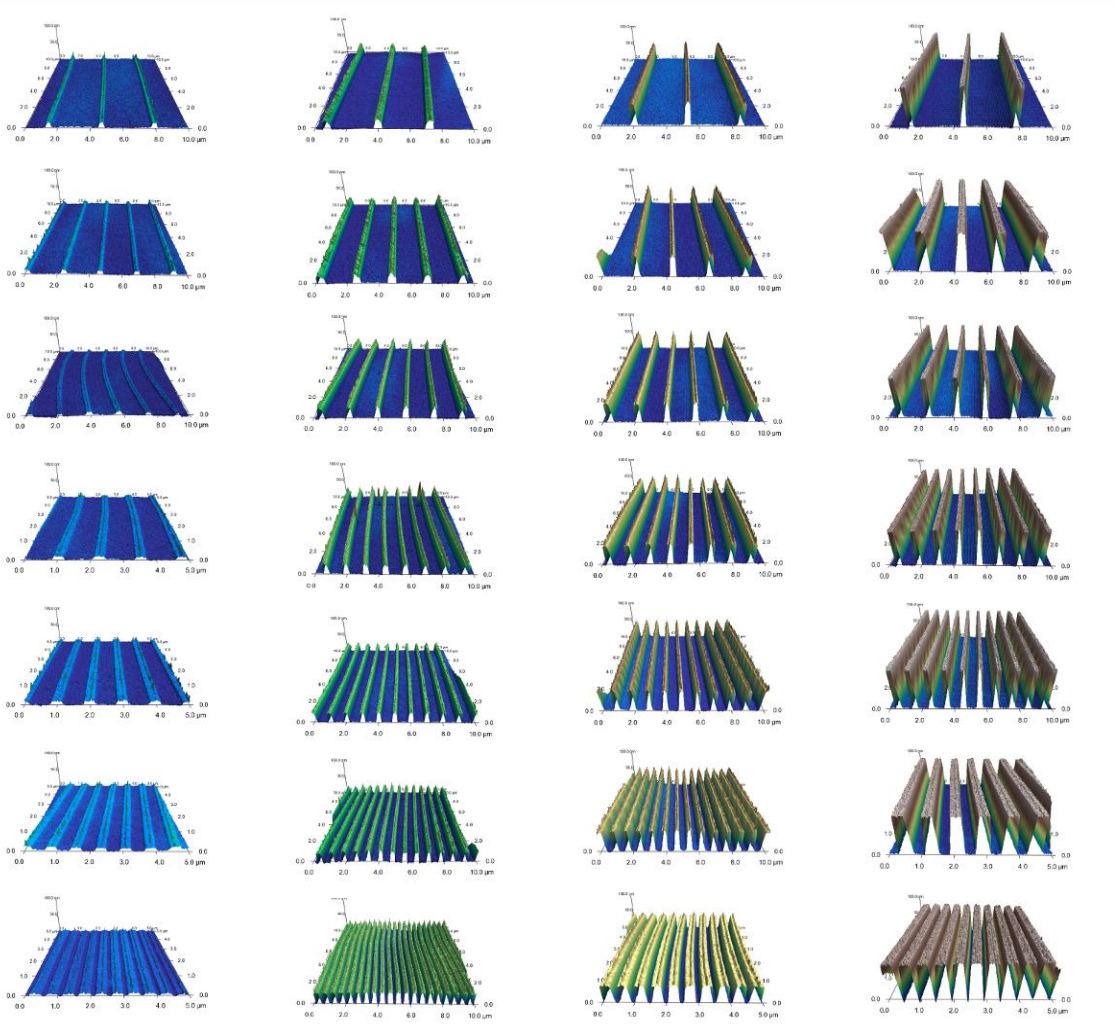

Figure 2.11 AFM height images of MA line gratings. Line heights of 10nm, 25nm, 50nm, and 95nm from left to right. The groove widths from top to bottom are 3µm, 2µm, 1.5µm, 1µm, 750nm, 500nm, and 250 nm.

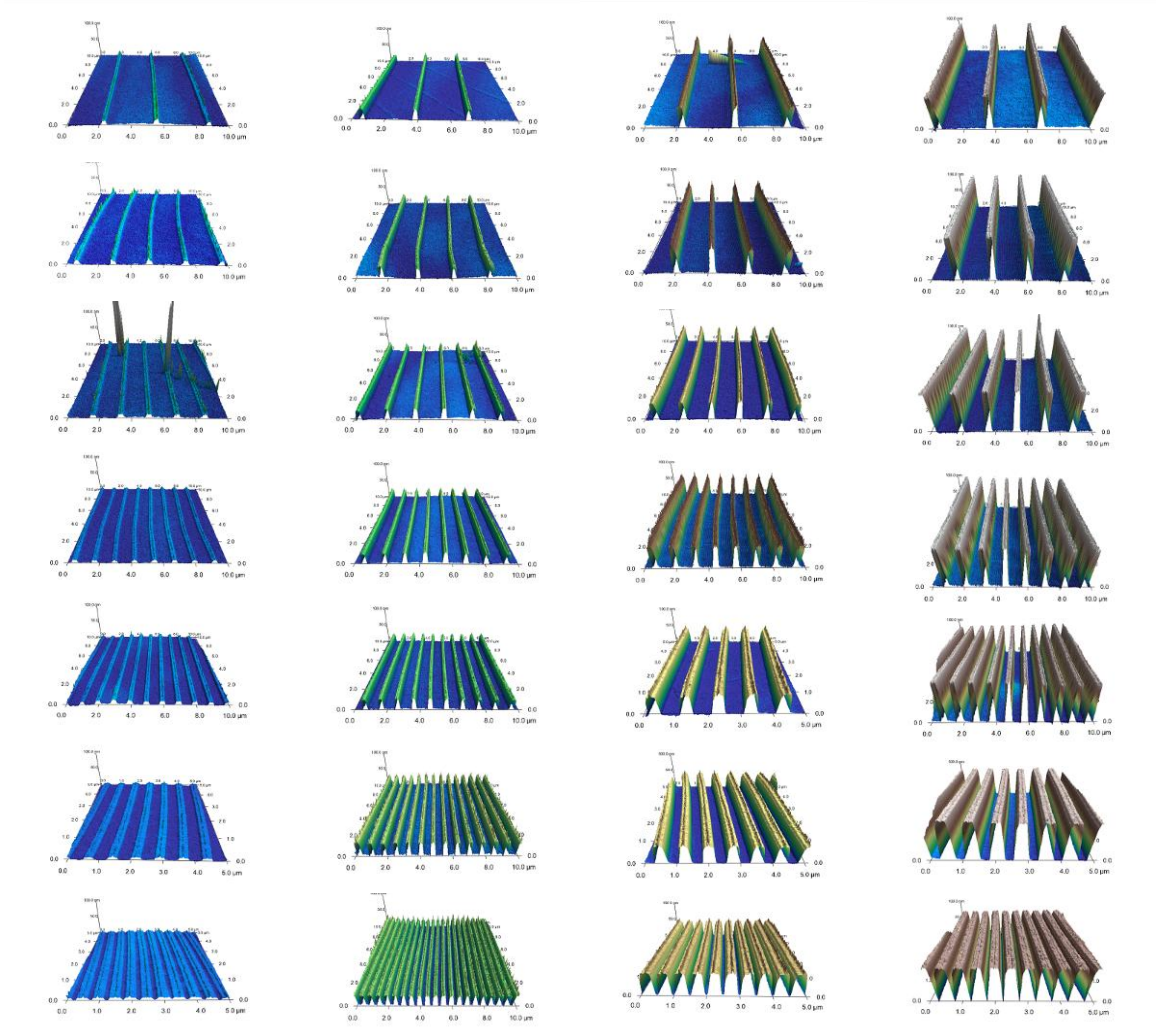

Figure 2.12 AFM height images of PU line gratings. Line heights of 10nm, 25nm, 50nm, and 95nm from left to right. The groove widths from top to bottom are 3μm, 2μm, 1.5μm, 1μm, 750nm, 500nm, and 250 nm.

References

(1) Berreman, D. W. *Molecular Crystals and Liquid Crystals* **1973**, *23*, 215.

(2) Berreman, D. W. *Phys. Rev. Lett.* **1972**, *28*, 1683-1686.

(3) Chiou, D. -.; Chen, L. -.; Lee, C. -. *Langmuir* **2006**, *22*, 9403-9408.

(4) Lin, R.; Rogers, J. A. *Nano Letters* **2007**, *7*, 1613-1621.

(5) Factor, B. J.; Russell, T. P.; Toney, M. F. *Macromolecules* **1993**, *26*, 2847-2859.

(6) Toney, M. F.; Russell, T. P.; Logan, J. A.; Kikuchi, H.; Sands, J. M.; Kumar, S. K. *Nature* **1995**, *374*, 709-711.

(7) Sakamoto, K.; Arafune, R.; Ito, N.; Ushioda, S.; Suzuki, Y.; Morokawa, S. *J. Appl. Phys.* **1996**, *80*, 431-439.

(8) Sakamoto, K.; Arafune, R.; Ito, N.; Usioda, S. *Jpn. J. Appl. Phys.* **1994**, *33*, L1323.

(9) Geary, J. M.; Goodby, J. W.; Kmetz, A. R.; Patel, J. S. *J. Appl. Phys.* **1987**, *62*, 4100-4108.

(10) O'Neill, M.; Kelly, S. M. *J. Phys. D* **2000**, *33*, R67-R84.

(11) Schadt, M.; Schmitt, K.; Kozinkov, V.; Chigrinov, V. *Jpn. J. Appl. Phys.* , *31*, 2155.

(12) Lee, J.; Lee, S.; Jeong, Y.; Cho, K. Y.; Park, J. *Opt. Express* **2009**, *17*, 23565-23575.

(13) Rolland, J. P.; Hagberg, E. C.; Denison, G. M.; Carter, K. R.; Simone, J. M. D. *Angewandte Chemie International Edition* **2004**, *43*, 5796-5799.

3. Multi-Stable Liquid Crystal Alignment Layers

3.1. Introduction

Liquid crystal alignment on surfaces is the subject of much research in both academia and industry. The ability to uniformly align liquid crystals is essential for LCD devices to operate properly. First generation displays required LC director alignment in only one direction, and rubbed polyimide films are typically used in such devices. Next generation devices may require more complicated director alignment modes, sub-pixel alignment, in conjunction with fabrication of multi-stable configurations, i.e. alignment layers which exhibit more than one stable orientation of azimuthal alignment. Multi-stable states allow the use of a pulsed electric field to turn the pixel on and off as opposed to keeping an electric field across the LCD cell for maintaining the "off" state as done in current LCDs. This will lead to a reduction in power usage, especially in computer monitors and static displays[1-6].

Theoretical modeling of this type of multi-stable alignment has been worked out by Fukuda et al, and others[7] for surfaces with four-fold and six-fold symmetry. The main conclusions from their work are that, for a fixed amplitude and periodicity of the surface pattern on the alignment layer, the (apolar) nematic director **n** will typically decide to align either 1) parallel to the periodic grooves on the surface (area (i) in the phase diagrams) or 2) at an angle bisecting the grooves (area (ii) in the phase diagrams), as shown in Figure 3.1. The orientation that is chosen is dependent on the elastic constants,

which are similar in nature to spring constants, of the liquid crystals. When you stretch, or deform, a spring along its axis the spring constant dictates the force required to stretch it. The LC director can be deformed in three dimensions, which creates multiple elastic constants (K_1 splay, K_2 twist, K_3 bend, and K_{24} saddle splay). In Figure 3.1, the phase diagrams are based on ratios of elastic constants. In this chapter we discuss LC director alignment on surfaces embossed with multiple degrees of symmetry-related alignment features, ranging from bi-stable square and rectangular features, four-fold symmetry, to tri-stable hexagonally-arrayed features, six-fold symmetry. We then examine an aperiodic Penrose pattern (Figure 3.2) with five-fold symmetry. The grooves that make up the sides of the rhombuses are at five unique angles, enabling long-range orientational order, but there is no long range translational order in the pattern.

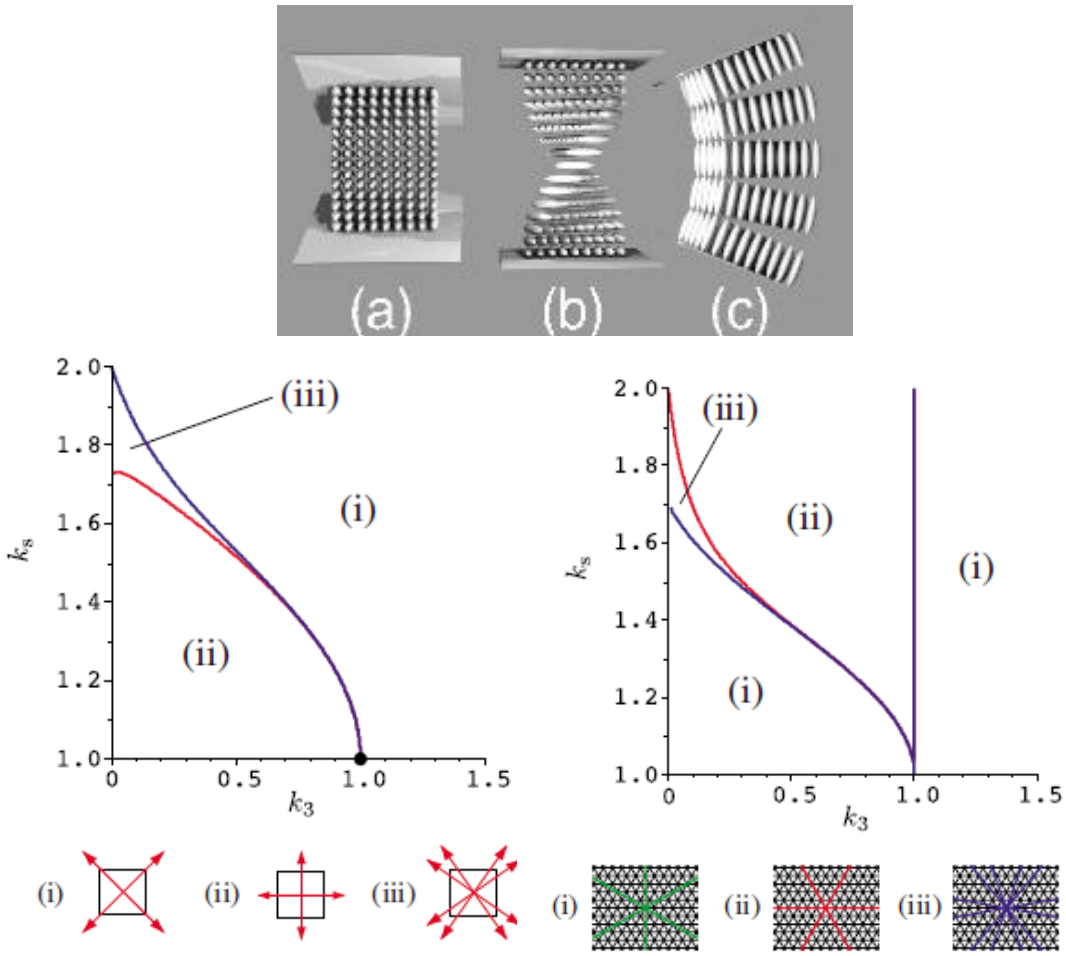

Figure 3.1 Schematic of LC constants and how they influence alignment on patterned surfaces. **Top:** Illustration of a) splay, b) twist, and c) bend elastic deformations.[8] **Bottom:** LC director orientation due to surface patterning as predicted by theory developed by Fukuda et al. for four-fold (left) and six-fold (right) symmetries. There are three sets of possible orientations, although one is highly improbable: i) bisecting the pattern and ii) parallel to the grooves. According to the Fukuda theory the elastic constants of the LC determines which alignment is chosen. The variables plotted are ratios of elastic constants.

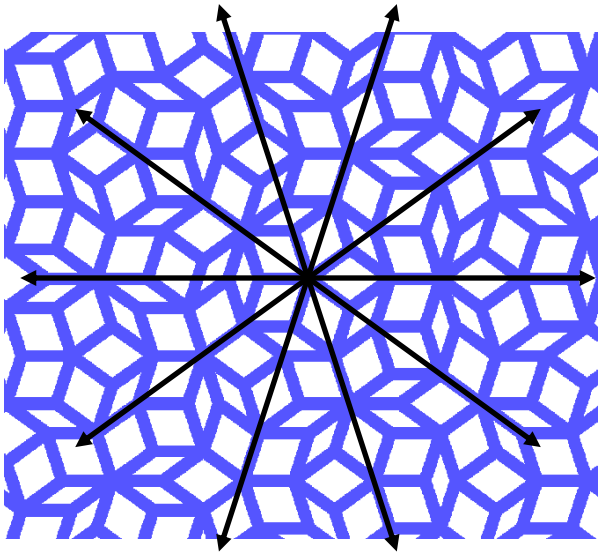

Figure 3.2 Orientation of grooves on Penrose pattern, black arrows. While no rotational or translational symmetry is present, the orientations of the grooves persist throughout the pattern. The theory has not been extended to such a pattern, but presumably the influences observed in the square and triangular patterns will be operative and enable us to qualitatively interpret the observations.

3.2. Experimental details

3.2.1. Materials

Glass substrates were cleaned by sequential sonication in soapy water, acetone, and isopropanol for 10 minutes each, dried with nitrogen, and stored in an oven at 110°C. Silicon wafers were purchased from Silicon Quest. Norland optical adhesive 73, polyurethane, was used as received. PFPE prepolymer formulation OAE-01 from Liquidia Technologies, Inc. was used with added DEAP photoinitiator.

3.2.2. Instrumentation

AFM images were captured with an Asylum MFP 3D, POM images were captured with an Olympus BX-61 polarized light setup.

3.2.3. Alignment Layers via PRINT

The fabricated masters were used as templates to fabricate patterned polymer films by a soft lithography method called PRINT as shown in Chapter 2 Figure 2.2. PFPE liquid oligomeric precursor was drop cast onto a template, cured with UV light under nitrogen gas for 3 minutes, and then removed from the template. PU precursor solution was drop cast onto glass cover slips, the mold applied with pressure from a roller, and exposed to UV light for 5 minutes.

3.2.4. LC device fabrication

In the previous chapter the orientation of the top and bottom alignment layer were parallel to one another creating a LC film with a single orientation of its director. In this chapter we fabricate devices using two different alignment layers. The bottom alignment layer is rubbed PI and the top alignment layer is embossed PU. The two alignment layers are

oriented such that rubbing direction on the bottom of the cell is perpendicular to one of the patterned grooves of the embossed pattern on the top of the cell.

3.3. Results and Discussion

3.3.1. AFM of Alignment Layers

AFM height images of embossed PU films show good fidelity to the template as shown in Figure 3.3. The triangles, squares, and rectangles are about 100nm tall while the Penrose a periodic patterns with five-fold symmetry are about 70 nm tall.

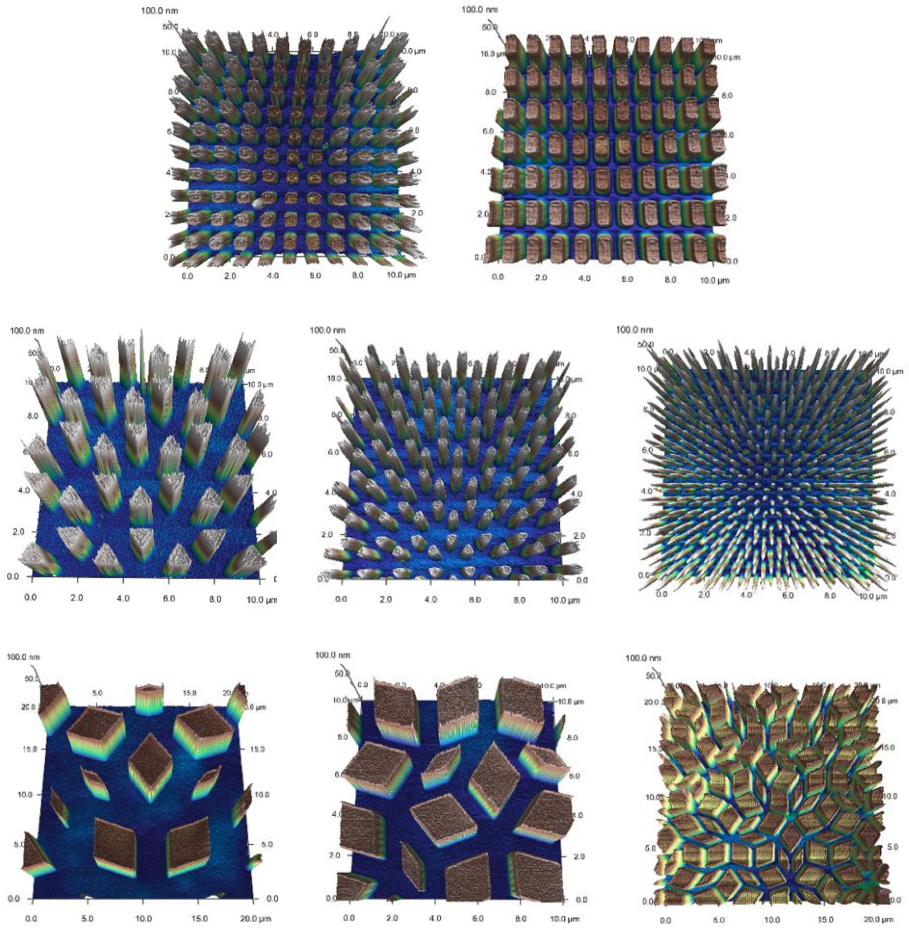

Figure 3.3 AFM height images of multi-stable patterns: **Top:** 500nm squares with 500nm groove widths and widths.1µm x 500nm rectangles with 500nm groove width, **Middle:** triangles with 1µm, 500nm, and 250nm side lengths and groove widths, **Bottom:** Penrose patterns with 3µm, 1µm, and 500nm groove widths. Square, rectangle, and triangle patterns are ~100nm tall, Penrose patterns are ~70nm tall.

3.3.2. POM

PU alignment layers were embossed on 0.2 mm thick microscope coverslips and paired with a rubbed PI film on the bottom of the cell (1x1" glass slide). The rubbing direction was aligned such that it was perpendicular to one groove direction for the triangles[99], squares, and Penrose patterns and perpendicular to the long axis of the rectangles. The rubbing direction was then aligned perpendicular to the polarizer and the analyzer was rotated from its crossed position in order to measure the twist of the director from the unidirectionally-rubbed PI cell bottom to the patterned (square, rectangle, triangle, or Penrose) top in the LC cell as illustrated in Figure 3.4.

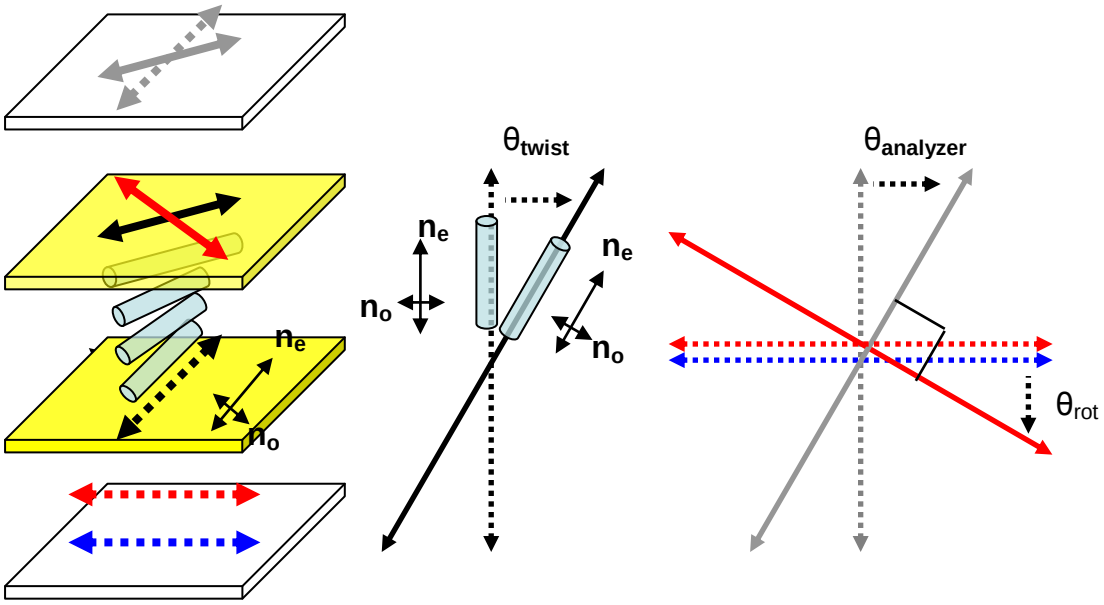

Figure 3.4 Schematic of device configuration for measuring the orientation of the LC director caused by the patterned top surface of the cell. Device structure on left, from bottom to top: unpolarized light passes through the polarizer (dashed blue arrow) and is transformed into linearly polarized light (dashed red arrow). The rubbing direction (dashed black arrow on rubbed PI, bottom of cell) is aligned parallel (or perpendicular) to the polarizer such that the polarized light is now aligned parallel with either $\mathbf{n_e}$ or $\mathbf{n_o}$, the indexes of refraction parallel to the long and short axis of the liquid crystal. As the LC director twists from bottom to the patterned top of the cell, the rotation of $\mathbf{n_e}$ and $\mathbf{n_o}$ causes the linearly polarized light to rotate (solid red arrow). In the above example the polarized light is initially parallel to $\mathbf{n_o}$, and remains parallel to $\mathbf{n_o}$ as the LC director rotates. The twist angle can be measured by rotating the analyzer (grey arrows) from the crossed position (dashed grey arrows) until it is perpendicular to the linearly polarized light exiting the device (solid grey arrows) indicated by a dark state, i.e. a dark state is achieved when $\theta_{analyzer} = \theta_{rot}$, as shown in the vector diagram on the right.

3.3.2.1. Square and Rectangular Alignment Patterns

POM images of the square pattern in Figure 3.5 show LC orientations at 45° and -45°, corresponding to the diagonals of the square pattern. At 10x magnification, the macroscopic alignment appears uniform and the boundaries between macroscopic domains with different twist angles (45° and -45° see Figure 3.5) are smooth. At 100x and with digital magnification, it is clear the boundary follows in detail the rectilinear pattern in a pixilated manner (See red squares on Figure 3.5). The distinct line at the boundary between orientations is caused by a thin wall of LC that is transitioning from a clockwise (+45°) to counter-clockwise (-45°) twist of the director from the bottom to top of the cell. At the point where the LC layer exhibits no twist (0°), a dark line is observed under crossed polarizers, because the LC director is oriented perpendicular to the analyzer, similar to the behavior of the line gratings in chapter two. As the analyzer is rotated this line becomes bright with a maximum intensity at 90°; the polarizer, linearly polarized light, and analyzer are all parallel at this point.

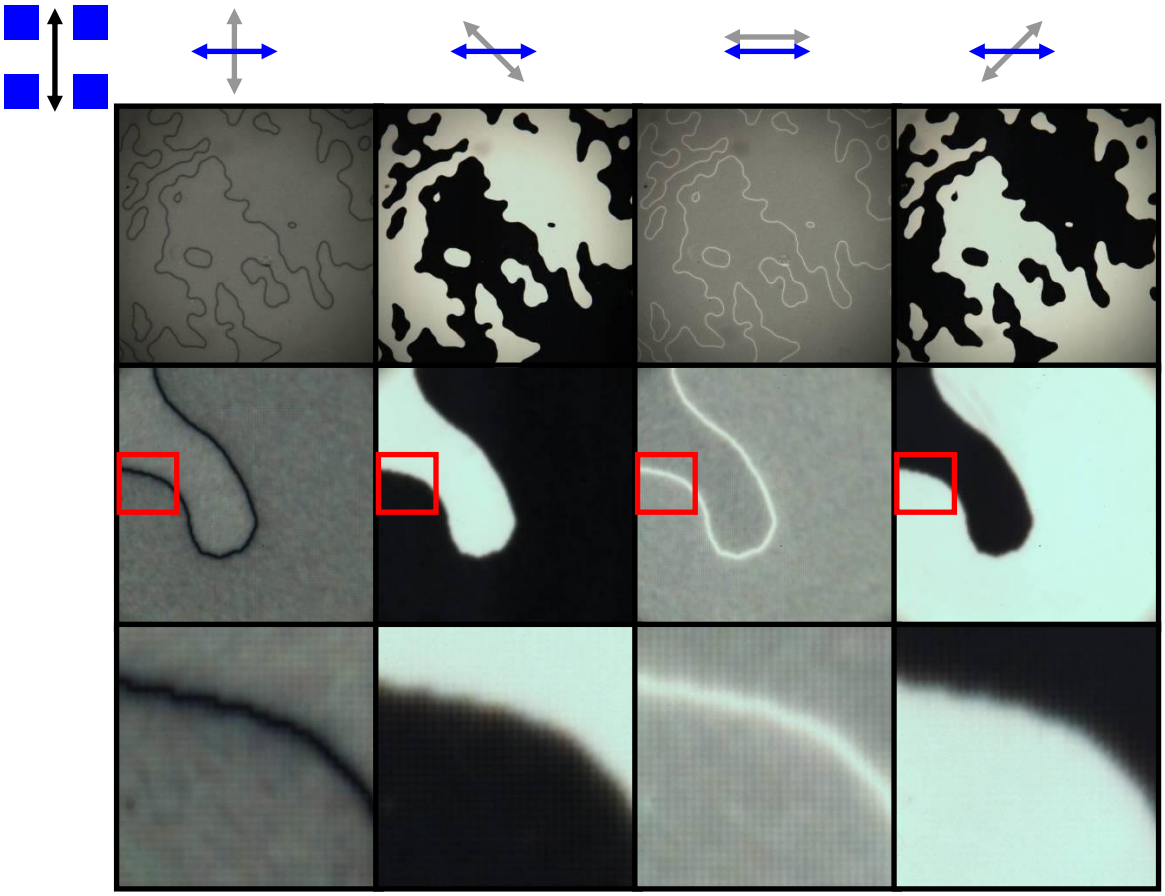

Figure 3.5 POM images of 100nm tall, 500nm groove width square pattern. Blue squares represent orientation of the square pattern and the black arrow represents the rubbed PI orientation. The blue arrow is the polarizer and the grey arrow is the analyzer orientation. From left to right, the analyzer is rotated 0°, -45°, 90°, and 45°. From top to bottom the images are taken at 10x, 100x, and digital zoom of area outlined by the red boxes.

Images of the rectangle patterned top cell substrate in Figure 3.6 show similar behavior except that the major director orientations are now ~+60° and -60°, corresponding to the diagonals of the patterned rectangular features. A similar LC wall at the boundary is observed indicating the transition between twist directions. At 10x magnification, the macroscopic alignment appears uniform and the boundaries between macroscopic domains with different twist angles (60° and -60°) are smooth. At 100x and with digital magnification, it is clear the boundary follows in detail the rectilinear pattern in a pixilated manner (See red squares on Figure 3.6), similar to what is seen with the square pattern.

The mechanism of director alignment on an array of square posts proposed in the literature[5] states that the diagonal is the average of the (orthogonal) director orientations in the surface grooves that propagates into the bulk LC layer as shown in Figure 3.7. This is also observed in our devices. The square pattern exhibits two director orientations one at +45° the other at -45°, and in the case of the rectangular pattern, we find two director orientations at +60° and -60° relative to the rubbed PI orientation. This would correspond to area (i) of the four-fold symmetry phase diagram predicted by Fukuda et al.[7], as shown in Figure 3.1.

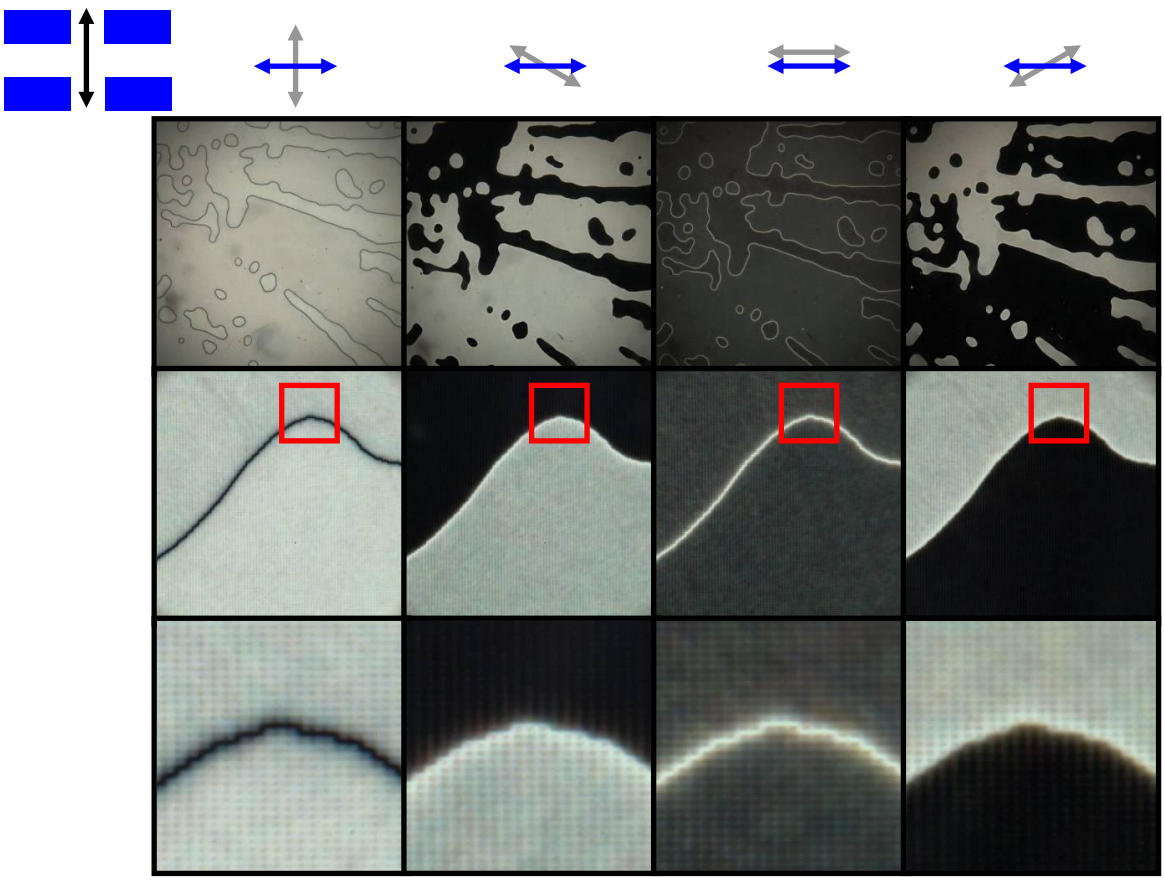

Figure 3.6 POM images of 100nm tall, 500nm groove width rectangle pattern. Blue rectangles represent orientation of the square pattern and the black arrow represents the rubbed PI orientation. The blue arrow is the polarizer and the grey arrow is the analyzer orientation. From left to right, analyzer rotated 0°, -60°, 90°, and 60° from the crossed position. From top to bottom the images are taken at 10x, 100x, and digital zoom of area outlined by the red boxes.

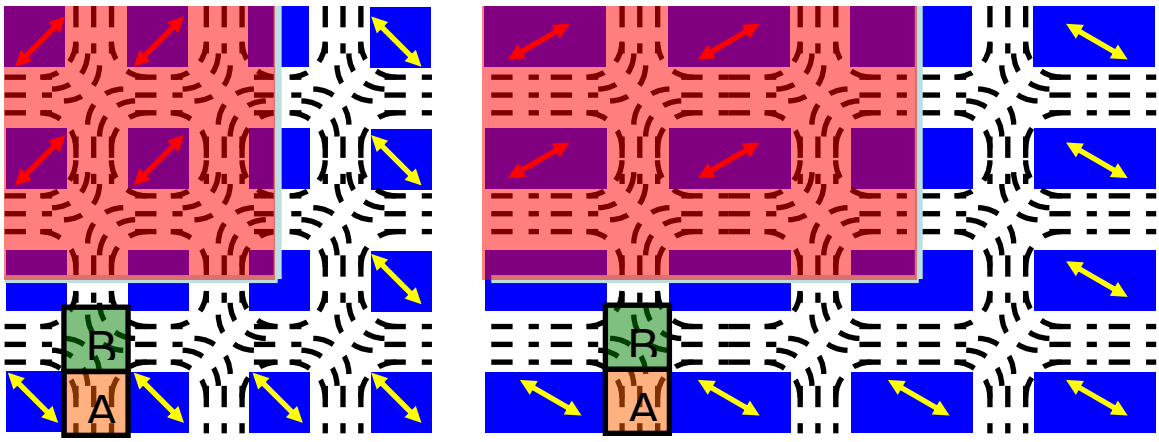

Figure 3.7 Schematic of LC director orientation on square and rectangular patterned surfaces. The dashed line represents localized LC director orientations, the red and yellow arrows represent long-range LC director orientations. At the surface the LC director aligns parallel to the walls of the pattern in between parallel faces, area A. Area B assumes an orientation that averages the orientation of the grooves, i.e. the diagonals of the pattern, 45° for the squares and ~60° for the rectangles. Different domains will choose to follow one diagonal versus the other as represented by the red and yellow arrows.

3.3.2.2. Triangular Alignment Patterns

If Fukuda's theory is correct, it is unclear whether a surface with six-fold symmetry should align parallel to the grooves or the bisecting angle, since areas (i) and (ii) of the six-fold symmetry plot overlaps with area (ii) of the four-fold symmetry plot in Figure 3.1. The device imaged for Figure 3.8 was made from a 1µm groove width triangular pattern with ~800nm tall features in combination with a rubbed PI alignment layer; there was no spacer determining the thickness of the LC layer. As a result, the alignment displayed by this device is dominated by the surface of the pattern. This is the case because the thickness of the LC film is of the same order of magnitude as the height of the pattern itself, i.e., the LC is essentially contained in the grooves of the triangular pattern with minimal material above the pattern before it encounters the rubbed polyimide surface. Rotation of the analyzer, -30°, 30°, and 90° from the crossed position revealed three different orientations of the LC director, each parallel to a groove direction in the patterned alignment layer. The zoomed image (Figure 3.8) helps to visualize the relationship between the embossed pattern and the LC domains of varying director orientations. The area between two parallel facing walls of a pair of triangles aligns the liquid crystal director parallel to the walls or along the grooves defining the pattern as illustrated in the schematic in Figure 3.9. The hexagonal centroid area in the triangle pattern is not directly influenced by the walls of the triangles, but is influenced by the oriented domains of LC surrounding the centroid and typically one such domain dictates the director orientation in that region. In the schematic, the black areas control the alignment in the hexagonal region. It is also evident from the POM image that even though one orientation is influencing LC alignment in the hexagonal region, the other LC orientations are still present. The simultaneous presence of three director orientations affects

the quality of the appearance of the macroscopic alignment as evidenced in the 10x images from Figure 3.8; it is apparent that while the majority of a domain may appear dark, bright spots associated with director alignment between remain very visible. Apparently the 1μm area between opposing triangle faces control the director orientation locally leading to the appearance of these bright spots. A LC wall at the boundaries is observed indicating the transition between twist directions, similar to what was observed in the square patterned devices.

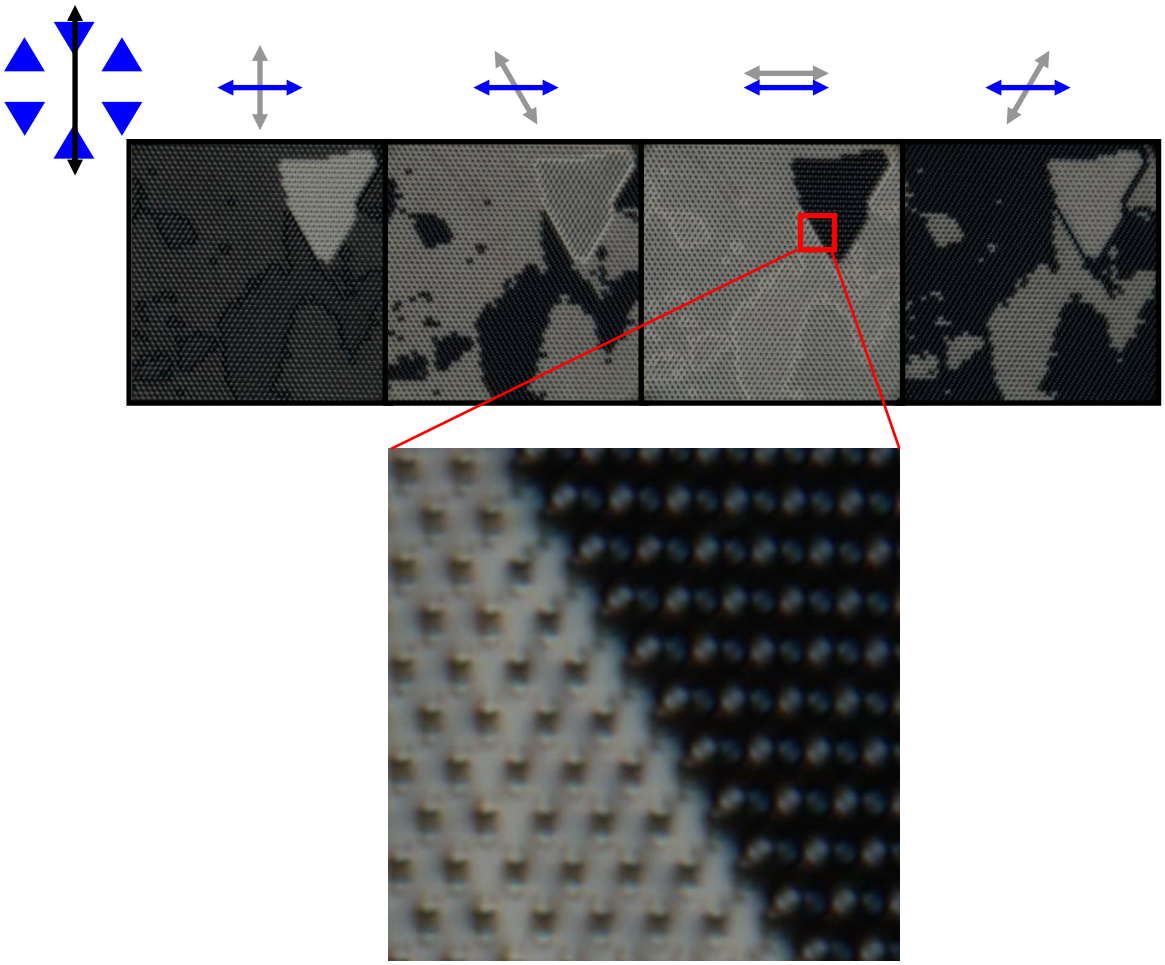

Figure 3.8 POM images of 800nm tall, 1μm triangles with analyzer rotated, from left to right, 0°, -30°, 90°, and 30° from the crossed position, polarizer is the blue arrow and analyzer is the grey arrow. These angles correspond to the orientation of the LC director in different domains. The zoomed in image shows the hexagonal array of triangles as well as the three different domains present.

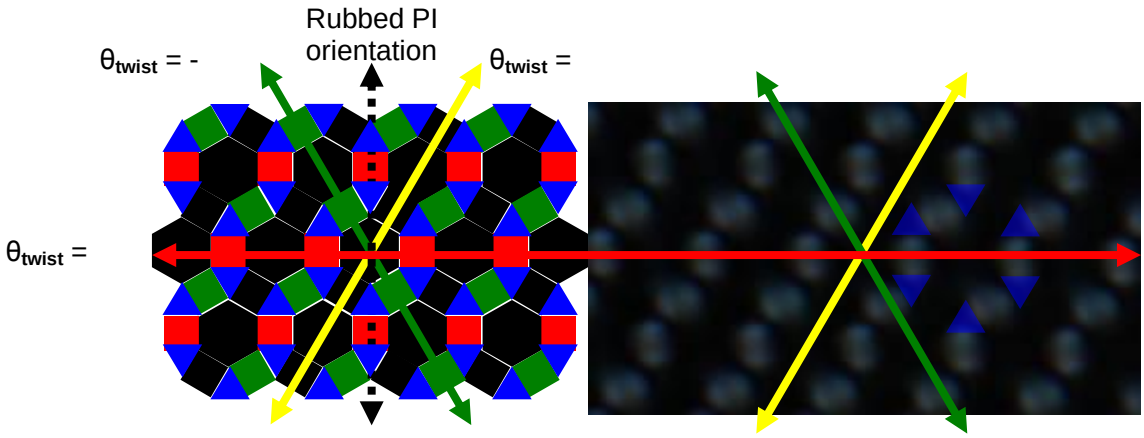

Figure 3.9 Schematic of liquid crystal alignment domains on a triangular pattern. (left) The square regions between two parallel faces of triangles are fixed in alignment, θ_{twist} = -30° for the green, θ_{twist} = 90° for the red, and θ_{twist} = 30° for the black regions, whereas the hexagonal area in the center of a hexagonal formation of triangles arbitrarily chooses to align with one of the fixed orientations, in this case θtwist = 30°, and dictates the macroscopic orientation of the liquid crystal layer. **Right:** POM image of 1μm triangles that are ~800nm tall, coupled with a rubbed PI substrate and analyzer rotated 150° from crossed position.

For the remaining triangular devices the height of the patterned features is reduced to ~100nm and its influence is further attenuated because 5µm polymer bead spacers are used to maintain a fixed thickness of the LC film above the features. This should minimize the bright spots, since the bulk of the LC thickness is above the features and is able to more strongly influence the director above surface areas of fixed director orientation. This also provides a way to determine if the ratio of pattern height to LC layer thickness influenced the orientation of the LC director, i.e. parallel to the grooves or the bisecting angle. Figure 3.10 contains POM images of the 100nm tall, 1µm groove width triangular pattern. The device displays only two orientations of the LC director, +30° and -30°, with respect to the rubbed PI orientation. A possible explanation for the absence of the 90° orientation of the LC director is that the elastic energyis higher for a twist of 90° versus 30°. In the 100nm feature height device, the LC film is much thicker than the pattern features and the director is able to select the lowest elastic energy state. Whereas, the 800nm tall triangular device was dominated by the surface pattern features, anchoring the LC director so that any alignment grooves that are 90° to the rubbed PI are trapped in that high energy orientation and unable to overcome the boundary conditions and adopt the lower energy orientations, +/- 30°. At 10x magnification, the macroscopic alignment appears uniform and the boundaries between macroscopic domains with different twist angles (+30° and -30° see Figure 3.10) are smooth. At 100x and with digital magnification, it is clear the boundary follows in detail the triangular pattern in a pixilated manner (See magnified red regions on Figure 3.10). The bright spots observed for the 800nm tall pattern are not visible at 10x magnification for the 100nm tall features, but are still observed at100x plus magnifications, indicating an increase in optical uniformity compared to the 800nm tall, 1µm groove width trianglular device. A

inversion wall at the boundaries is observed, indicating the transition between twist directions, similar to what was observed in the square patterned devices.

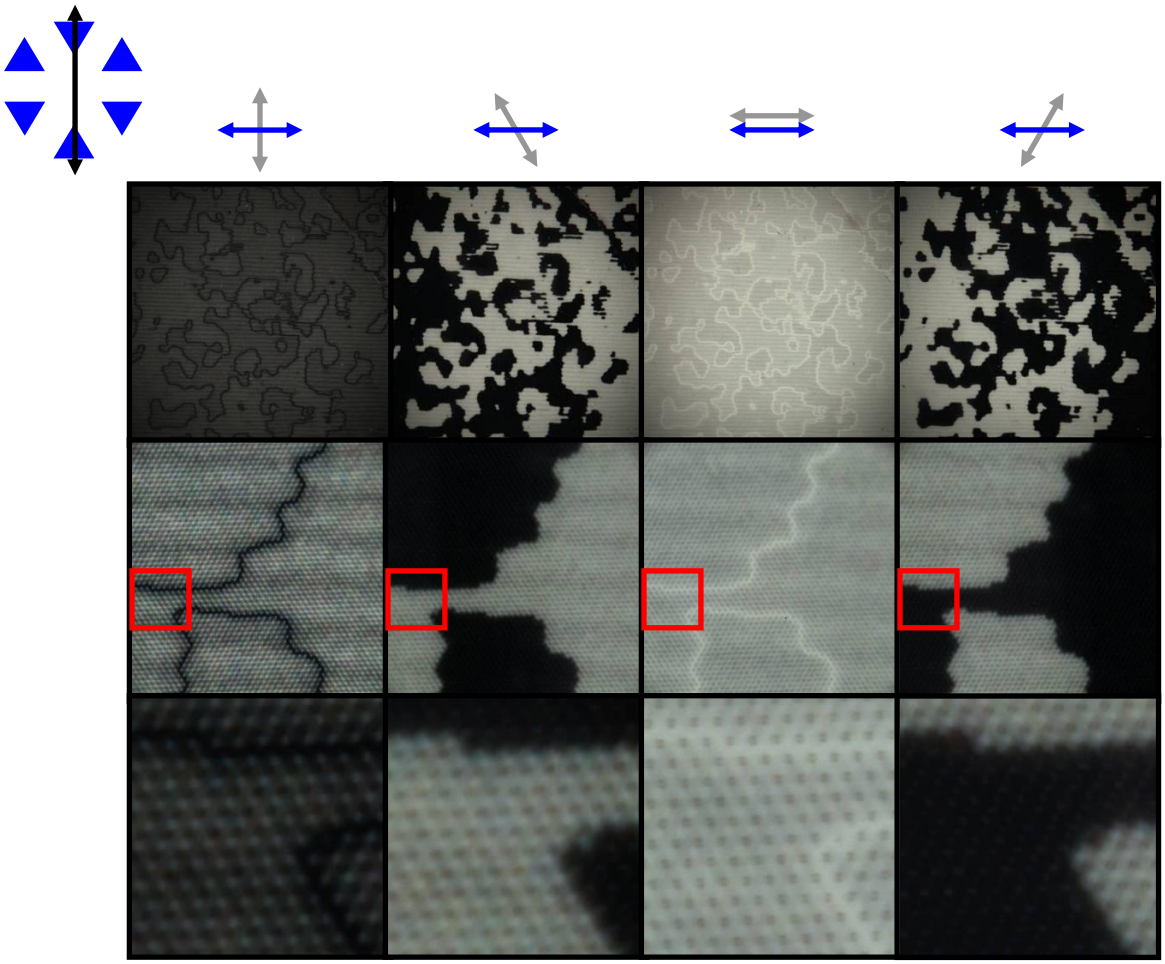

Figure 3.10 POM images of 100nm tall, 1um groove width trianglular pattern, from left to right, analyzer rotated 0°, -30°, 90°, and 30° from the crossed position. From top to bottom the images are taken at 10x, 100x, and digital zoom on area outlined by the red boxes. A dark state at $\theta = 0$ was difficult to find in these devices.

The liquid crystal response to the 100nm tall, 500nm groove width triangular pattern shown in Figure 3.11 also only exhibits two director orientations at 30° and -30°. At 10x magnification, the macroscopic alignment appears uniform and the boundaries between macroscopic domains with different twist angles (+30° and -30° see Figure 3.9) are smooth. At 100x and with digital magnification, it is clear the boundary follows in detail the triangular pattern in a pixilated manner (See red squares on Figure 3.11).The bright spots observed in 1μm groove width devices are no longer visible at any magnification and the inversion at the boundaries is observed indicating the transition between twist directions, similar to what was observed in the square patterned devices.

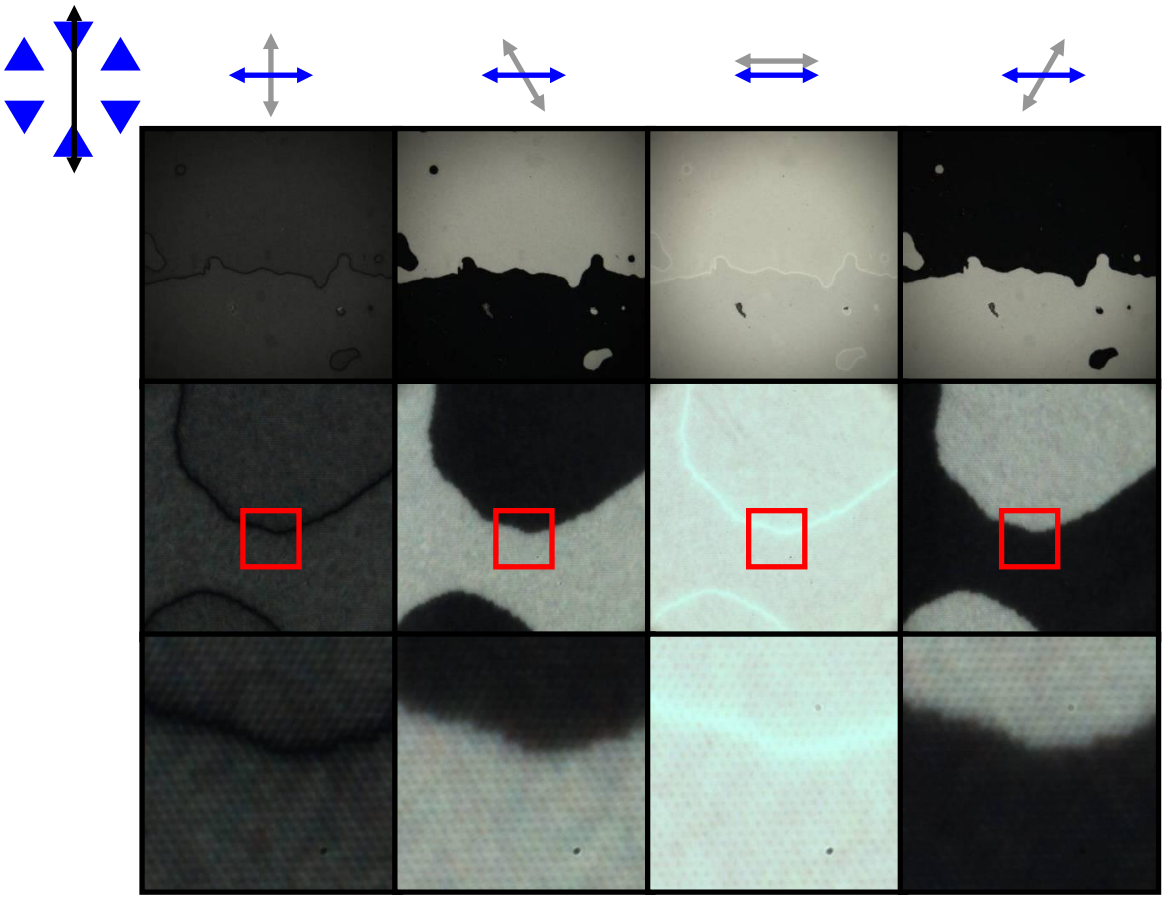

Figure 3.11 POM images of 100nm tall, 500nm groove width trianglular pattern, from left to right, analyzer rotated 0°, -30°, 90°, and 30° from the crossed position. From top to bottom the images are taken at 10x, 100x, and digital zoom on area outlined by the red boxes. The boundaries are much smoother and the alignment is more optically uniform at higher magnification than the 1µm triangle pattern due to a decrease in the domain size between triangle faces. A dark state at $\theta = 90°$ was difficult to find in these devices.

POM images of devices made with the 250nm groove width triangular pattern, shown in Figure 3.12, mainly exhibit one director orientation at 15°, with some areas exhibiting a director orientation at 0°. This indicates the director is mainly orienting parallel to the rubbed PI hence the triangle pattern is effectively exhibiting planar degenerate alignment and the features exhibit no anchoring bias. This means the patterned surface aligns LCs parallel to the substrate, but the azimuthal orientation follows the more strongly aligning substrate, in this case rubbed PI. This may be due to the small dimensions of the domain size, ~250nm x 250nm for this pattern, which are unable to influence the hexagonal centroid areas more strongly than the rubbed PI. The walls of the triangle pattern are also not completely flat, as seen in Figure 3.2, due to the limitations of the photolithographic process that was used to fabricate the master.

The mechanism of director alignment on a hexagonal array of triangular posts has not been proposed in the literature, but it should be straight forward to apply conclusions from square and rectangular patterns. As previously stated, Fukuda's theory offers no real prediction for the triangular pattern based on the results for the square pattern. In the hexagonal array of triangular features the director aligns parallel to the grooves, at -30°, +30°, and 90° with respect to the rubbed PI orientation. Figure 3.13 shows a schematic of the LC director orientations on the triangular patterned surface. The LC director aligns parallel to triangle walls, similar to the square pattern, and attempts to curve around a corner. As it does this the director rotates through orientations that are parallel to all three groove orientations. This allows the LC director in the hexagonal centroid to align parallel to one of the groove directions. Based on the POM images, we believe the boundary follows a fairly complicated pattern as shown in Figure 3.13.

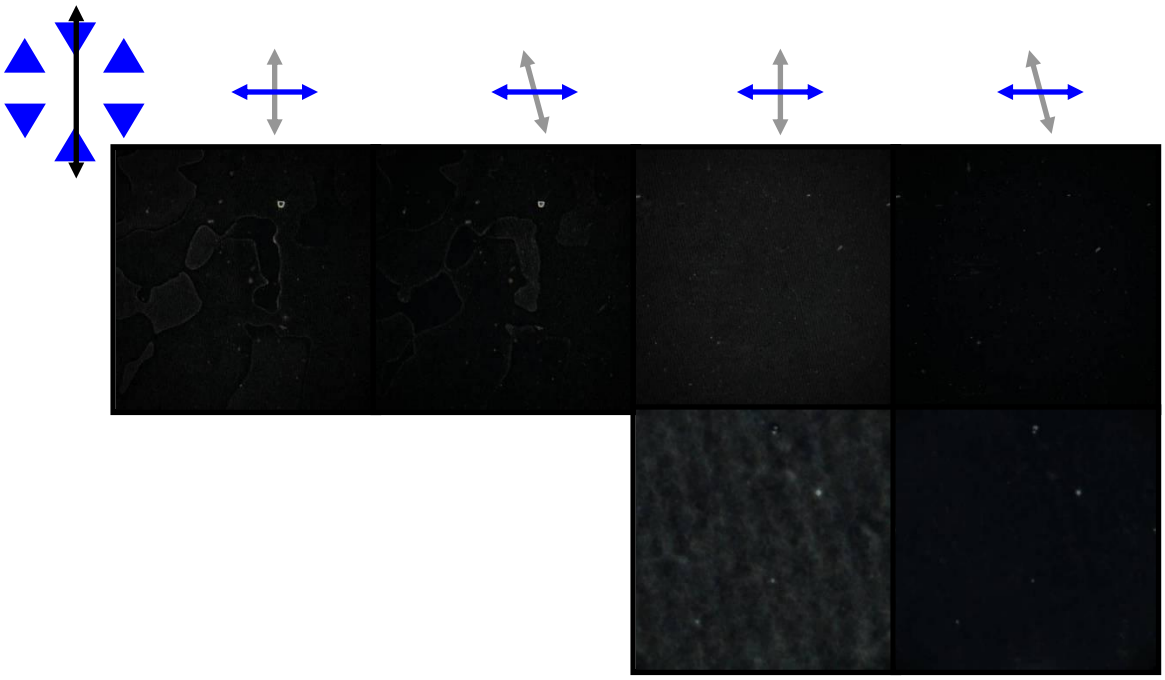

Figure 3.12 POM images of 100nm tall, 250nm groove width trianglular pattern, from left to right, analyzer rotated 0°, -15°, 0°, and -15° from the crossed position, polarizer is the blue arrow and analyzer is the grey arrow. From top to bottom the images are taken at 10x, 100x. The two images on the top left show two domains of LC alignment that differ in orientation by ~15 degrees. The small twist angles indicate that the triangle pattern is not strongly influencing LC alignment and is exhibiting some planar degenerate qualities, meaning it duplicates the alignment of the rubbed PI substrate.

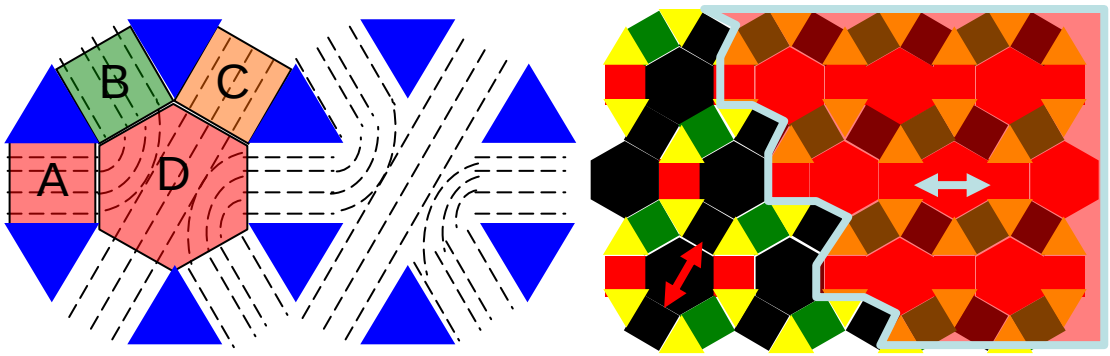

Figure 3.13 Schematic of localized LC directors and the boundary between two director orientations at the surface of triangular patterned surfaces. Based on POM images, the LC director above the top of the triangles to follow the orientation of the LC director in the hexagonal centroid.

3.3.2.3. Penrose Patterns

The hexagonal array of triangle features increased the complexity of director alignment options from bistable orthogonal options to tri-stable patterns. We were interested to see how an aperiodic pattern would influence alignment. Penrose patterns arise from nonperiodic tiling of a surface with an aperiodic set of prototiles which sometimes exhibit five-fold symmetry. In our work, the pattern is based on two rhombuses with different angle sets. Traditional five-fold symmetry is not present; however, the grooves forming the rhombuses are oriented at five different angles creating a type of broken symmetry, as shown in Figure 3.2. The grooves in the devices studied are located at 90°, +54°, +18°, -18°, and -54° with respect to the rubbed PI. Figure 3.14 shows POM images of 3μm groove width Penrose tiling devices. Only two macroscopic orientations of LC director were observed at -18° and +18° at 10x magnification. Small domains of LC directors oriented in other directions were apparent making the optical uniformity quite poor compared to what was observed on the previous patterns. At 100x magnification, we observe that LCs align parallel to the walls of the rhombohedral features and that even though macroscopic alignment is observed, the mixture of alignment domains observed at high magnification suggest the contrast ratio of such a device would be quite low. The digital zoom shows distant dependent LC orientation parallel to the walls of the features, i.e. the further from the walls the more susceptible the LC director is to other aligning influences.

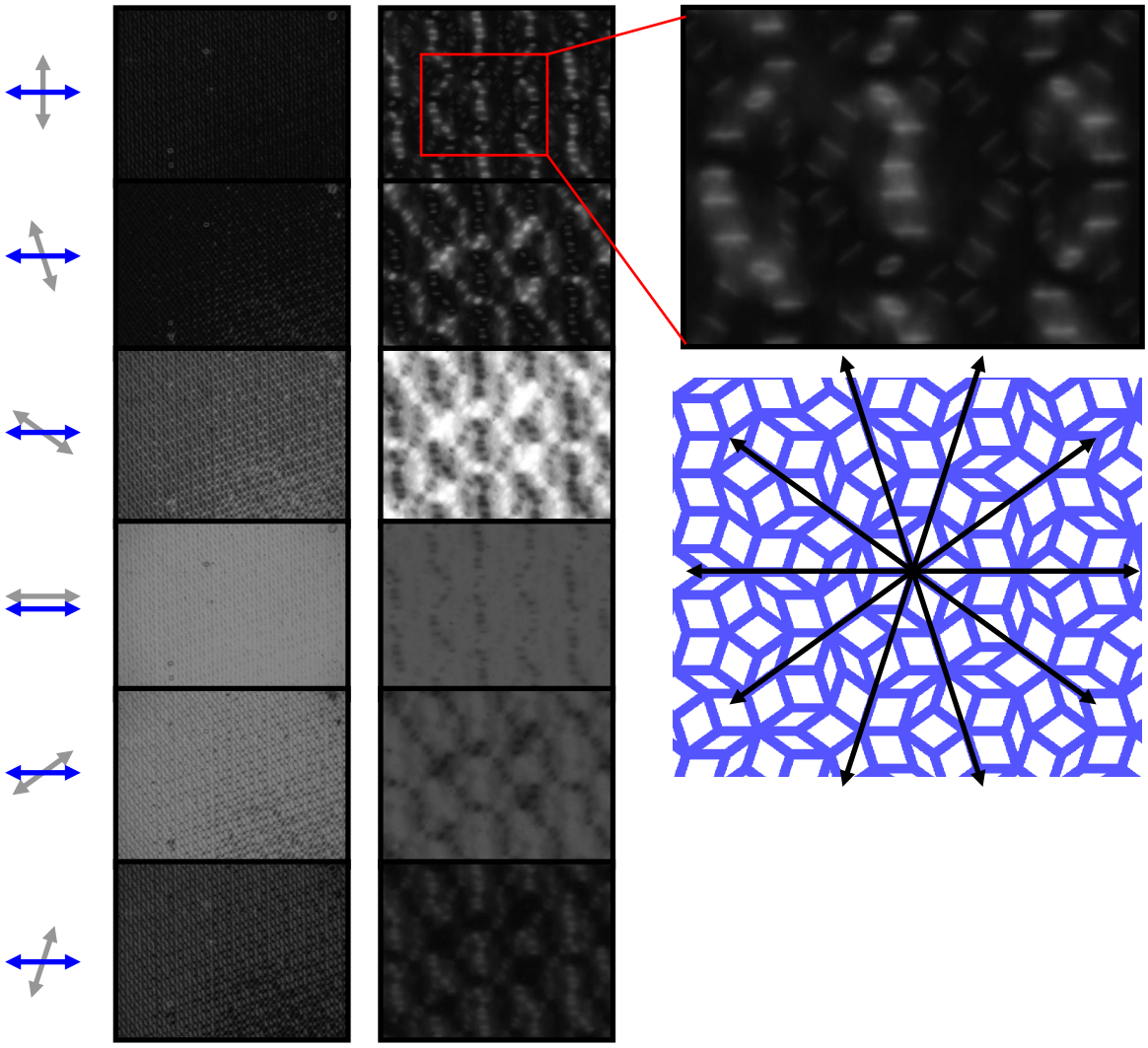

Figure 3.14 POM images of 70nm tall, 3 µm groove width Penrose pattern, from top to bottom, analyzer rotated 0°, -18°, -54°, -90°, 54°, and 18° from the crossed position. From left to right the images are taken at 10x and 100x. Macroscopic alignment is observed with two twist angles observed at +18° and -18°, but the optical uniformity is quite low, especially at higher magnification. Digital zoom, red box, of the device viewed with crossed polars reveals how the LC directors are initially oriented parallel to the walls of the rhombuses and then follow the macroscopic alignment further into the grooves.

Figure 3.13 shows 1μm groove width pattern. At 10x magnification, five macroscopic LC director orientations are observed parallel to the grooves, as expected; however, at 100x magnification, it is still obvious that these domains consist of a mixture of smaller domains oriented in different directions. There appear to be wandering snakelike domains which may correspond to parts of the Penrose pattern where the faces of the rhombuses are able to reinforce a given alignment, i.e. the faces of the rhombuses along these domains are oriented parallel to one another. Figure 3.14 shows the 500nm groove width pattern. These devices behave in the same manner as the 1μm devices in that, at 10x magnification, five macroscopic LC director orientations are observed parallel to the grooves, and at 100x magnification, it is still obvious that these domains consist of a mixture of smaller domains oriented in different directions. The snakelike domains are smaller and more difficult to resolve, but this is because the feature size of the patterns are smaller.

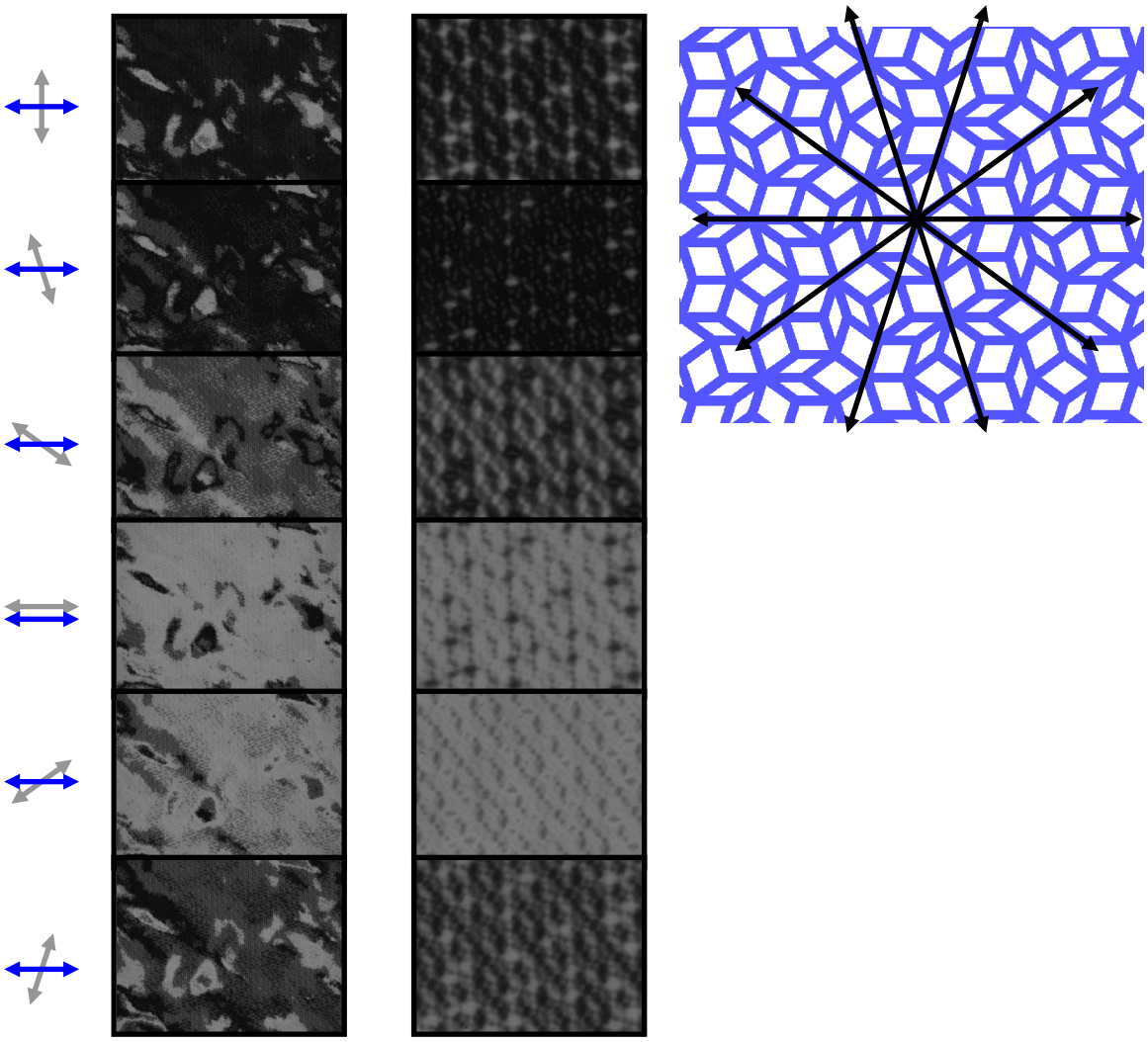

Figure 3.15 POM images of 70nm tall, 1 µm groove width Penrose pattern, from top to bottom, analyzer rotated 0°, -18°, -54°, -90°, 54°, and 18° from the crossed position. From left to right the images are taken at 10x and 100x. Five twist angles are observed in this device corresponding to the orientations of the lines in the pattern.

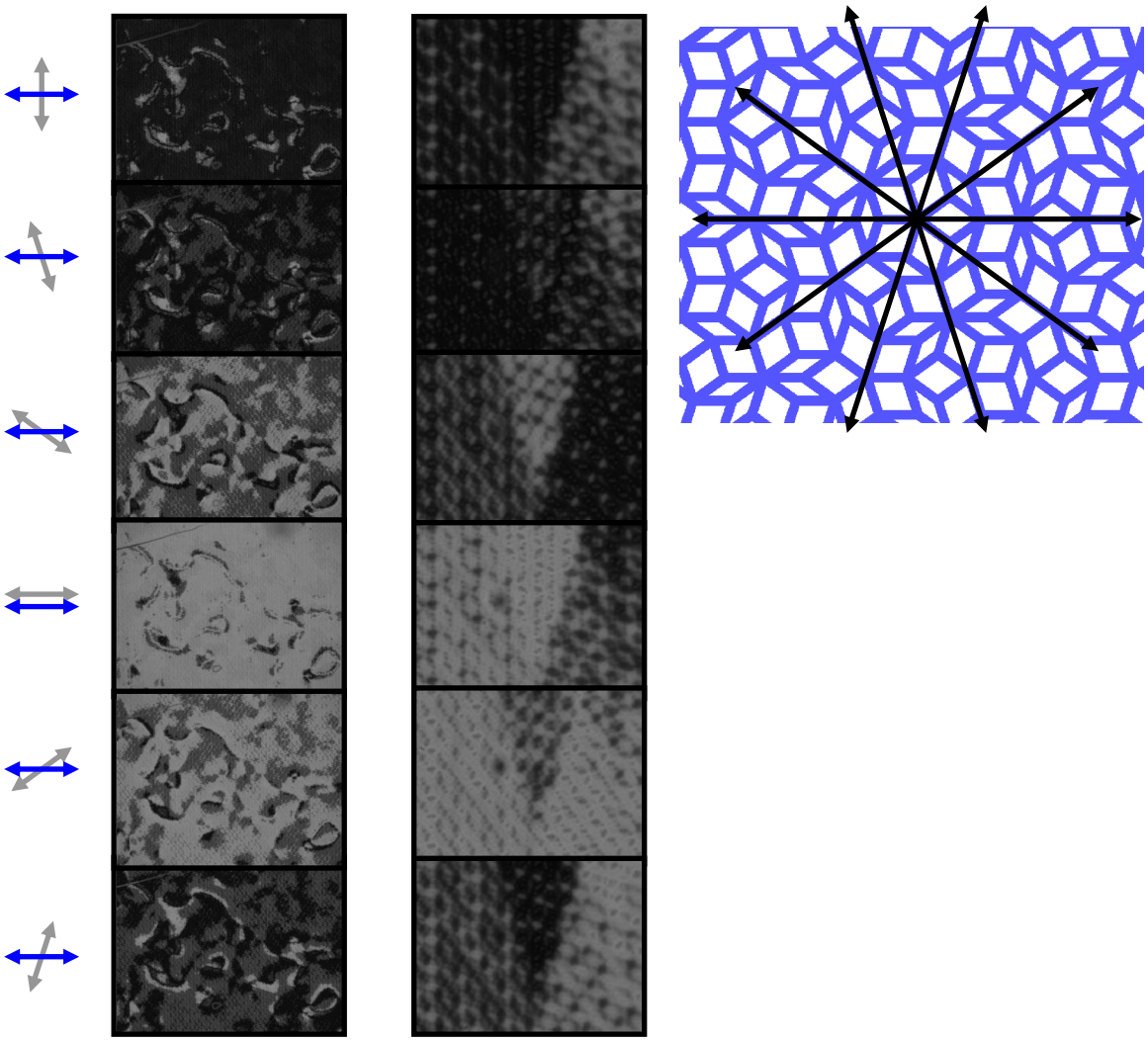

Figure 3.16 POM images of 70nm tall, 500nm groove width Penrose pattern, from top to bottom, analyzer rotated 0°, -18°, -54°, -90°, 54°, and 18° from the crossed position. From left to right the images are taken at 10x and 100x. Five twist angles are observed in this device corresponding to the orientations of the lines in the pattern.

3.4. Conclusions

Multi-stable LC alignment was observed on square, rectangle, triangle, and Penrose patterned PU surfaces. In the LC domains between two parallel, vertical faces of the pattern features, the director is aligned parallel to the vertical face of the pattern and the bottom of the groove. These micro-domains of LC alignment are oriented at various angles depending on the symmetry of the pattern. These local domains then compete to orient the LC on a macroscopic. The square and rectangle patterns aligned LCs in a manner predicted by theory and previous experiments. Theory predicting the orientation of 1μm and 500nm groove width triangular patterns was unspecific. 250nm groove width triangular patterns yielded planar degenerate alignment due to a decrease in micro-domain size. The Penrose patterns exhibited multi-stable alignment parallel to the grooves, despite the broken symmetry of the pattern. Micro-domain sizes of ~500nm x 500nm displayed the best optical uniformity by creating domains near the size of the average wavelength of light while maintaining adequate LC alignment strength.

References

(1) Gwag, J. S.; Kim, J.; Yoneya, M.; Yokoyama, H. *Appl. Phys. Lett.* **2008**, *92*, 153110.

(2) Kim, J.; Yoneya, M.; Yamamoto, J.; Yokoyama, H. *Appl. Phys. Lett.* **2001**, *78*, 3055-3057.

(3) Niitsuma, J.; Yoneya, M.; Yokoyama, H. *Appl. Phys. Lett.* **2008**, *92*, 241120.

(4) Thurston, R. N.; Cheng, J.; Boyd, G. D. *IEEE Transactions on Electronic Devices* **1980**, *27*, 2069.

(5) Yi, Y. W.; Khire, V.; Bowman, C. N.; Maclennan, J. E.; Clark, N. A. *J. Appl. Phys.* **2008**, *103*, 093518.

(6) Yi, Y.; Nakata, M.; Martin, A. R.; Clark, N. A. *Appl. Phys. Lett.* **2007**, *90*, 163510.

(7) Fukuda, J.; Gwag, J. S.; Yoneya, M.; Yokoyama, H. *Phys. Rev. E* **2008**, *77*, 011702.

(8) Anonymous
Overview of the mesoscopic theory of liquid crystals. *http://wwwitp.physik.tu-berlin.de/muschik/liquid_crystals/lc_intro.html*.

(9) Alkhairalla, B.; Allinson, H.; Boden, N.; Evans, S. D.; Henderson, J. R. *Phys Rev E.* **1999**, *59*, 3033-3039.

4. Microfabrication Procedures

4.1. Introduction

Microfabrication techniques have been an integral part in the development of consumer electronics by facilitating the fabrication of integrated circuits (ICs) and micro-electromechanical systems (MEMS). They are also being applied to advance current research in materials science, chemistry, physics, engineering, and biology. Microfabrication techniques include controlled deposition of materials, photolithography, and etching.[1] Because of the sensitivity of these techniques to dust, temperature, and humidity they are typically done in clean rooms. [2]

4.1.1. Vapor Deposition

There are two types of vapor deposition, chemical vapor deposition (CVD)[3], and physical vapor deposition (PVD)[4]. CVD is a chemical process used to produce high-purity, high-performance solid materials. The process is often used in the semiconductor industry to produce thin films. In a typical CVD process, the wafer (substrate) is exposed to one or more volatile precursors, which react and/or decompose on the substrate surface to produce the desired deposit. Frequently, volatile by-products are also produced, which are removed by gas flow through the reaction chamber. CVD is used to deposit materials in various forms, including: monocrystalline, polycrystalline, amorphous, and epitaxial. These materials include: silicon, carbon fiber, carbon nanofibers, filaments,

carbon nanotubes, SiO2, silicon-germanium, tungsten, silicon carbide, silicon nitride, silicon oxynitride, titanium nitride, and various high-k dielectrics. PVD is a general term used to describe any of a variety of methods to deposit thin films by the condensation of a vaporized form of the material onto various surfaces (e.g., onto semiconductor wafers). The coating method involves purely physical processes such as high temperature vacuum evaporation or plasma sputter bombardment.

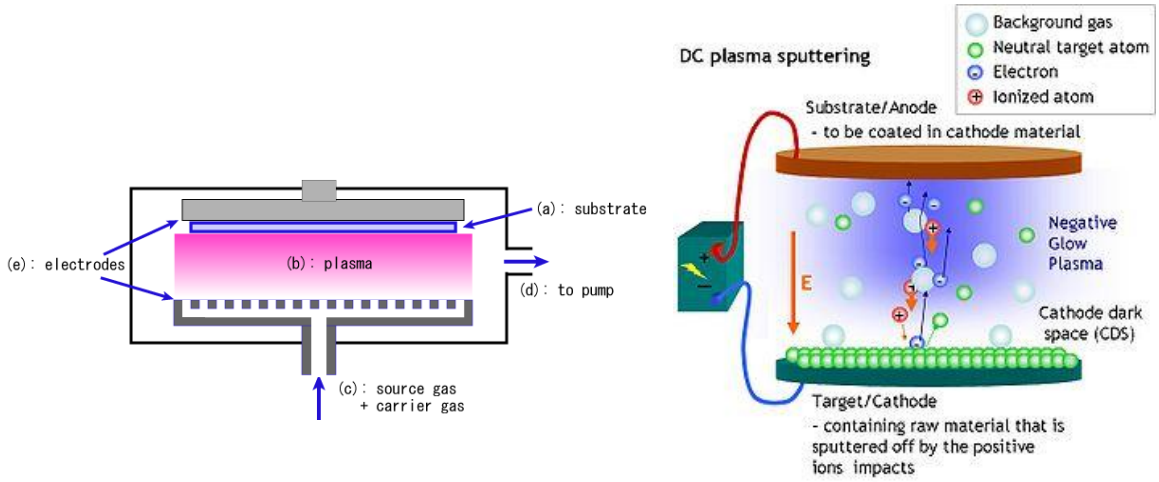

Figure 4.1 CVD and PVD schematics. **Left:** Schematic of CVD chamber. In this type of CVD, plasma is used to enahnce the chemical reaction of the precursor materials. **Right:** Schematic of sputter PVD: plasma is used to physically remove atoms from a target material that is then deposited onto a substrate at a controlled rate. [3, 4]

4.1.2. Photolithography

Photolithography, is a process used to selectively remove parts of a thin film or the bulk of a substrate. It uses light to transfer a geometric pattern from a photo mask to a light-sensitive chemical photo resist, or simply "resist," on the substrate. A series of chemical treatments then engraves the exposure pattern into the material underneath the photo resist, as described in more detail in the etching section and Figure 4.2. In complex integrated circuits, for example a modern CMOS, a wafer will go through the photolithographic cycle up to 50 times.[5]

4.1.3. Etching

Etching is the process which transfers the pattern from the resist into the substrate. There are two important figures of merit in these processes: selectivity and isotropy. Selectivity refers to the ratio of etch rates of the substrate versus the resist. Isotropy refers to the direction in which the etchant removes the substrate as shown in Figure 4.3. There are two types of etching processes: wet and dry. In wet etching, liquid acids or bases are used. Selectivity and isotropy are controlled by changing the chemistry, temperature, and exposure time of the etchant. Dry etching employs halogenated plasmas at low pressure to remove material. Selectivity and isotropy are controlled by chemistry, gas pressure, power used to generate the plasma, and exposure time. Dry etching typically yields higher anisotropy than wet etching.[6]

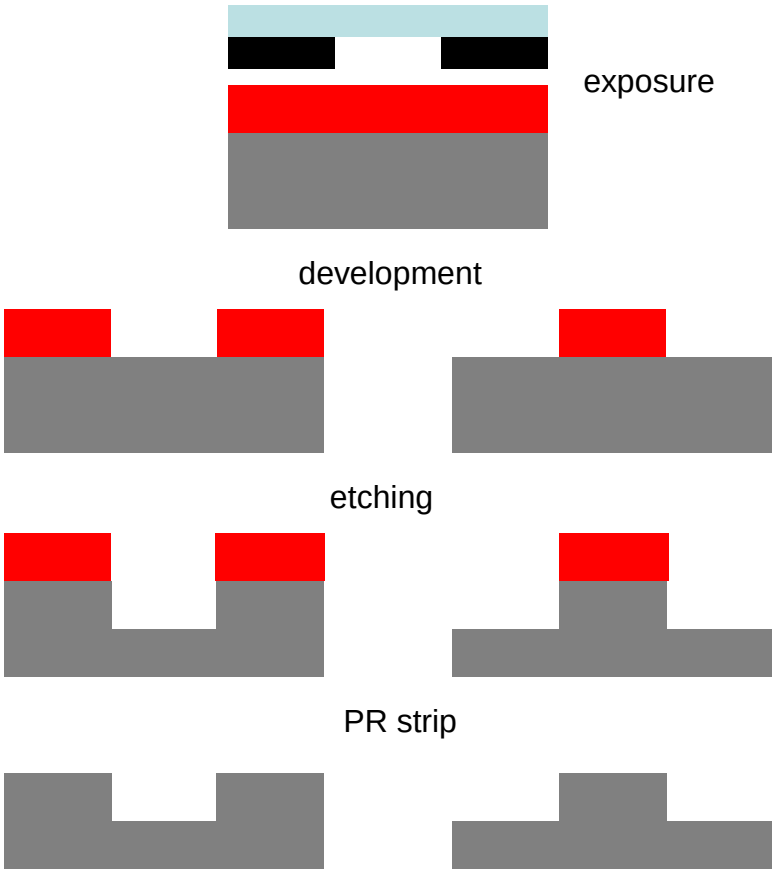

Figure 4.2 Schematic of the photolithography process. A photo-resist (PR), red, is exposed with light that is passed through a patterned mask. Depending on the nature of the material the area exposed to light either stays or is removed by a developer. The pattern is then etched into the substrate and the PR is removed.

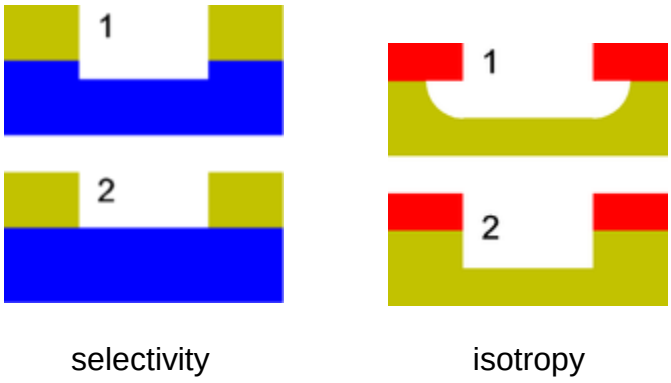

Figure 4.3 Schematic of selectivity and isotropy
Left: Yellow: layer to be removed; blue: layer to remain
1. A poorly selective etch removes the top layer, but also attacks the underlying material.
2. A highly selective etch leaves the underlying material unharmed.
Right: Red: masking layer; yellow: layer to be removed
1. A perfectly isotropic etch produces round sidewalls.
2. A perfectly anisotropic etch produces vertical sidewalls. [6]

4.2. Experimental

4.2.1. Materials

Chrome on quartz reticules were fabricated by Benchmark Technologies according to the specifications we provided and used with no modifications. Chrome on glass photomasks were fabricated by Infinite Graphics and used as provided. Silicon wafers were purchased from Silicon Quest and used as provided. ITO coated glass slides were purchased from Delta technologies and sequentially sonicated in soapy water, acetone, and isoporpanol for 10 minutes, and dried with nitrogen. S1813 photoresist, adhesion propmoter, and developer was provided by CHANL and used as provided. Concentrated HCl was purchased from Fisher Scientific and diluted with deionized water at a 1:1 ratio.

4.2.2. Instrumentation

Wafer patterning was performed at the Triangle Nano Lithography Center at NCSU. Photolithography was done using a 193nm ASML scanner by Dave Vellenga. Plasmatherm RIE was used to etch the square, rectangle, triangle, line grating, and Penrose features of 150nm tall or less. DRIE was used to etch taller features. Asher oxygen plasma was used to strip the photoresist. ITO coated glass patterning was performed in the CHANL cleanroom at UNC using the mask aligner.

4.2.3. Silicon Master Fabrication

Dave Vellenga performed photolithography on the silicon wafers. Chlorine plasma was used to etch the silicon wafer and the photoresist was stripped by oxygen plasma. The etch time and power used to generate the plasma was adjusted to obtain patterns with varied feature heights as shown in Table 4.1. The photoresist was then stripped by oxygen plasma under the conditions listed in Table 4.1.

Table 4.1 RIE Processes

Process	BARC 70	40.10		40.50		40		100b		150		250	
Step	**1**	**1**	**2**	**1**	**2**	**1**	**2**	**1**	**2**	**1**	**2**	**1**	**2**
Time(s)	70	30	**40**	30	**40**	30	**40**	30	**100**	30	**150**	30	**250**
Pressure(mTorr)	40	15	15	15	15	15	15	15	15	15	15	15	15
Power(W)	50	100	**10**	100	**50**	100	**100**	100	100	100	100	100	100
Cl2(sccm)	0	20	20	20	20	20	20	20	20	20	20	20	20
O2(sccm)	8	0	0.6	0	0.6	0	0.6	0	0.6	0	0.6	0	0.6

4.2.4. Electrode Fabrication

Electrodes for multi-stable devices were fabricated following a thin film transistor configuration (TFT). Adhesion promoter was drop cast onto cleaned ITO coated glass slides and left for 10s, after which they were spun coat at 3k rpm for 40s and baked at 115°C for 60s. S1813 was then spun coat at 3k rpm for 40s and baked at 115°C for 60s. The mask aligner was then used in hard contact mode with 100μm spacing and 7.5s exposure followed by a 90s post-exposure bake. The exposed resist was developed for ~20s, rinsed with DI water, and dried with nitrogen. ITO was then etched in diluted HCl for 10 minutes, rinsed with DI water, and dried with nitrogen. It is anticipated that silicon nitride will be evaporated onto the patterned ITO, followed by sputtering of aluminum, which will undergo similar photolithography steps to fabricate the inter-digitated electrode illustrated in Figure 4.2.

4.3. Results and Discussions

Patterned silicon masters were successfully patterned with feature heights ranging from 10 to 800nm, as listed in Table 4.2 and Figure 4.4. Only the 250nm triangular pattern

exhibits defects from the photolithography process. There is rounding of the triangles due to the wavelength of light used to expose the photoresist being similar to the size of the pattern. RIE was useful to fabricate patterns of 200nm or less. Attempts to achieve taller features resulted in complete removal of the photoresist and redeposition onto the substrate, which in some cases coated the wafer with an insoluble polymer film. For taller features DRIE was required, but the 250nm triangles were completely removed by this process, i.e. no pattern remained. Patterning of ITO was straight forward, but there are possible problems with the process. The developers and photoresist are subject to degradation over time, and over exposure leads to less photoresist will remain after development. It is useful to perform quality control using a reflective optical microscope after developing the resist and a multi-meter was used to verify removal of ITO. It is also important to test all patterning parameters in a serial manner before attempting mass production.

Table 4.2 Patterned Silicon Wafer Dimensions and Patterns

Wafer ID	Feature Height(nm)	Feature Pattern
40.10	10	tri., rec., sq., line gratings
40.50	25	tri., rec., sq., line gratings
40	50	tri., rec., sq., line gratings
100b	95	tri., rec., sq., line gratings
250	200	tri., rec., sq., line gratings
45D	800	tri., rec., sq., line gratings
P40.50	25	Penrose, conc. circles
P100	70	Penrose, conc. circles
P150	120	Penrose, conc. circles

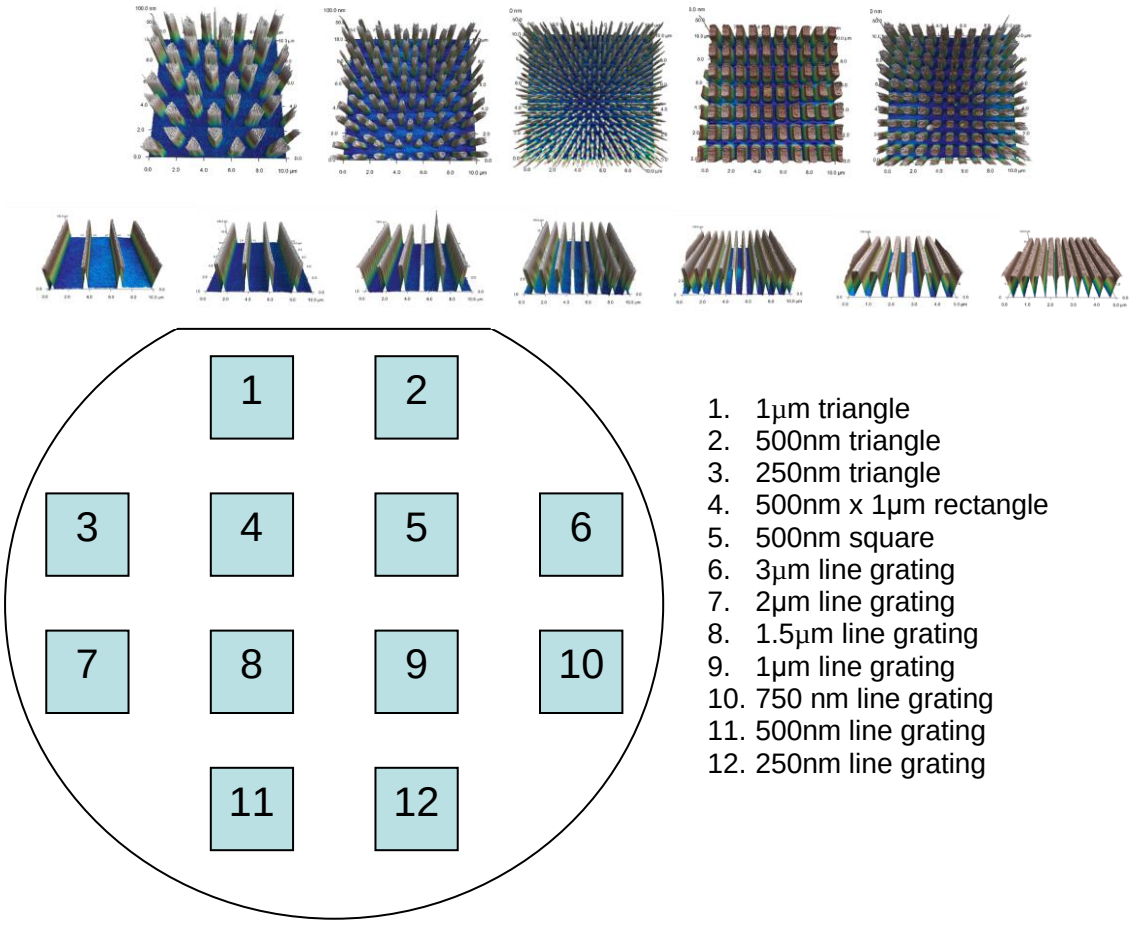

Figure 4.5 Wafer layout of etched patterns. Wafers with different feature heights were fabricated with the same layout, see Table 4.2 for more details.

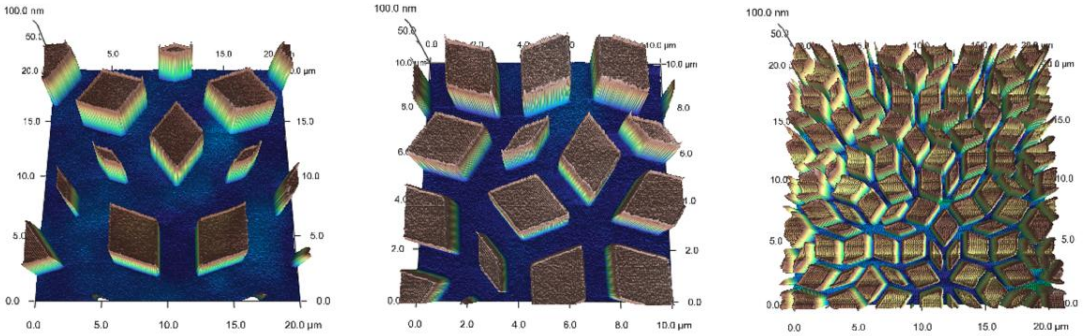

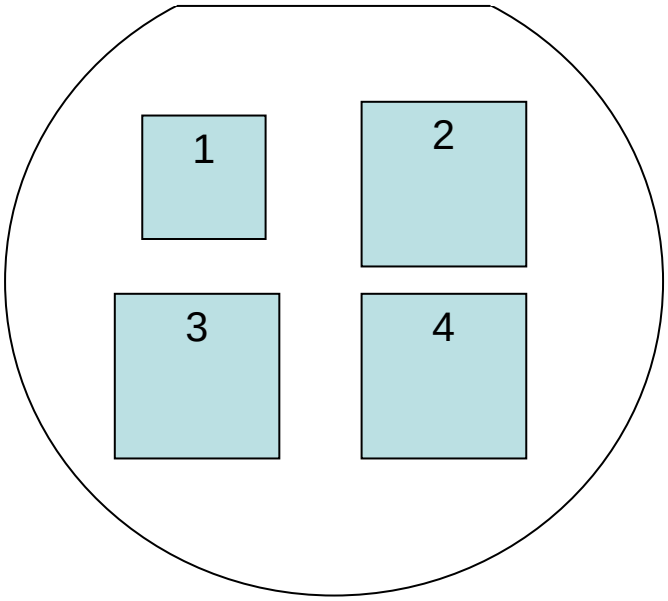

1. Array of concentric circles with 500nm duty cycle
2. 3μm groove width(left)
3. 1μm groove width(middle)
4. 500nm groove width(right)

Figure 4.6 Wafer layout of etched patterns. Wafers with different feature heights were fabricated with the same layout, see Table 4.2 for more details.

4.4. Conclusions

Microfabrication techniques developed by the semiconductor industry are useful in fabricating patterned silicon wafers as pattern templates for embossed polymer films. The features sizes accessible through these methods allow the study of mechanistically relevant LC alignment layers. The only downside to master fabrication using these methods is the tools utilized frequently require maintenance and repair which can be a major source of time delays.

References

(1) Anonymoushttp://en.wikipedia.org/wiki/Microfabrication. *http://en.wikipedia.org/wiki/Microfabrication*.

(2) Madou, M. J. In *Fundamentals of microfabrication : the science of miniaturization;* CRC Press: Boca Raton, 2002; .

(3) Anonymoushttp://en.wikipedia.org/wiki/Chemical_vapor_deposition. *http://en.wikipedia.org/wiki/Chemical_vapor_deposition*.

(4) Anonymoushttp://en.wikipedia.org/wiki/Physical_vapour_deposition. *http://en.wikipedia.org/wiki/Physical_vapour_deposition*.

(5) Anonymoushttp://en.wikipedia.org/wiki/Photolithography. *http://en.wikipedia.org/wiki/Photolithography*.

(6) Anonymoushttp://en.wikipedia.org/wiki/Etching_(microfabrication). *http://en.wikipedia.org/wiki/Etching_(microfabrication)*.